

Multi-Horizon Electricity Price Forecasting with Deep Learning in the Australian National Electricity Market

Mohammed Osman Gani^{a,b,*}, Zhipeng He^{a,b}, Chun Ouyang^{a,b}, Sara Khalifa^{a,b}

^a*School of Information Systems, Queensland University of Technology, Australia*

^b*Energy Transition Centre, Queensland University of Technology, Australia*

Abstract

Accurate electricity price forecasting (EPF) is essential for operational planning, trading, and flexible asset scheduling in liberalised power systems, yet remains challenging due to volatility, heavy-tailed spikes, and frequent regime shifts. While deep learning (DL) has been increasingly adopted in EPF to capture complex and nonlinear price dynamics, several important gaps persist: (i) limited attention to multi-day horizons beyond day-ahead forecasting, (ii) insufficient exploration of state-of-the-art (SOTA) time series DL models, and (iii) a predominant reliance on aggregated horizon-level evaluation that obscures time-of-day forecasting variation. To address these gaps, we propose a novel EPF framework that extends the forecast horizon to multi-day-ahead by systematically building forecasting models that leverage benchmarked SOTA time series DL models. We conduct a comprehensive evaluation to analyse time-of-day forecasting performance by integrating model assessment at intraday interval levels across all five regions in the Australian National Electricity Market (NEM). The results show that no single model consistently dominates across regions, metrics, and horizons. Overall, standard DL models deliver superior performance in most regions, while SOTA time series DL models demonstrate greater robustness to forecast horizon extension. Intraday interval-level evaluation reveals pronounced diurnal error patterns, indicating that absolute errors peak during the evening ramp,

*Corresponding author

Email addresses: mohammedosman.gani@hdr.qut.edu.au (Mohammed Osman Gani), zippo.he@qut.edu.au (Zhipeng He), c.ouyang@qut.edu.au (Chun Ouyang), sara.khalifa@qut.edu.au (Sara Khalifa)

relative errors inflate during midday negative-price regimes, and directional accuracy degrades during periods of frequent trend changes. Regional analysis highlights substantial variation in forecasting errors across the NEM, consistent with differences in regional generation portfolios and price distribution characteristics. These findings suggest that future research on DL-based EPF can benefit from enriched feature representations and modelling strategies that enhance longer-term forecasting robustness while maintaining sensitivity to intraday volatility and structural price dynamics.

Keywords: Electricity price forecasting, deep learning, time series forecasting, Australian National Electricity Market, day-ahead, two-day-ahead

Nomenclature

AEMO	Australian Energy Market Operator	MLP	Multilayer Perceptron
BESS	Battery Energy Storage System	MSE	Mean Squared Error
BiLSTM	Bidirectional Long Short-Term Memory	NEM	Australian National Electricity Market
CNN	Convolutional Neural Network	NSW	New South Wales
DL	Deep Learning	NYISO	New York Independent System Operator
ENTSO-E	European Network of Transmission System Operators for Electricity	PJM	PJM Interconnection LLC
EPF	Electricity Price Forecasting	QLD	Queensland
EPEX	European Power Exchange	rMAE	Relative Mean Absolute Error
ETT	Electricity Transformer Temperature	RMSE	Root Mean Square Error
GCN	Graph Convolutional Network	RRP	Regional Reference Price
GRU	Gated Recurrent Unit	S4	Structured State Space Model
ILI	Influenza-Like Illness	SA	South Australia
LR	Learning Rate	sMAPE	Symmetric Mean Absolute Percentage Error
LSTM	Long Short-Term Memory	SOTA	State-of-the-art
MAE	Mean Absolute Error	SSM	State Space Model
MAPE	Mean Absolute Percentage Error	TAS	Tasmania
MDA	Mean Directional Accuracy	VIC	Victoria
ML	Machine Learning	VRE	Variable Renewable Energy

1. Introduction

Electricity price forecasting (EPF) is fundamental to modern power systems, enabling optimised trading, asset scheduling, risk management, and enhanced system reliability. In liberalised and competitive electricity markets, the role of EPF becomes even more critical, as accurate EPF is integral to operational planning [1], investment decision-making [2], and renewable energy integration [3]. However, achieving accurate EPF remains challenging due to electricity prices exhibiting high volatility, sudden spikes, frequent regime shifts, nonlinearity, and non-stationarity, often driven by complex interactions among demand-supply conditions, market rules, and growing renewable penetration [4, 5]. As a result, electricity price time series are considerably more irregular and structurally complex than those in conventional financial or economic domains, leading to substantial forecasting challenges [6, 7]. The field has seen sustained research interest over the past three decades, driving the development of diverse forecasting approaches.

EPF research has evolved through two broad methodological paradigms: statistical approaches (e.g., [8, 9, 10, 11]) and machine learning (ML)-based approaches (e.g., [12, 13, 14, 15, 16, 17]). Early studies relied heavily on statistical and econometric models, which provided interpretable structures for modelling mean reversion, volatility, and periodicity through the representation of linear relationships and temporal dependencies [18]. However, the inherent complexity of modern liberalised electricity markets, characterised by high volatility, pronounced nonlinearity, and sudden price spikes, has increasingly limited the effectiveness of linear modelling approaches. In response, ML methods, and later deep learning (DL), emerged as dominant alternatives capable of capturing nonlinear behaviour and have been applied across a wide range of electricity markets. More recent studies have also explored hybrid models that integrate statistical rigour with ML and DL techniques, aiming to leverage the strengths of both paradigms [19].

Despite substantial progress, several important gaps remain in the existing EPF literature. *Firstly*, most studies focus on hour-ahead and day-ahead forecasting [20], often overlooking multi-day horizons such as two-day-ahead forecasting. However, multi-day horizons are essential for strategic planning and for operational tasks, for example, battery energy storage system (BESS) scheduling, which requires visibility across consecutive days to optimise resource allocation and manage risk arising from market volatility. *Secondly*, recent advances in general-purpose time series modelling, includ-

ing architectures designed for long-sequence learning and efficient temporal representation, have been largely overlooked in EPF research. As a result, it remains unclear whether these models, which have achieved state-of-the-art (SOTA) performance across diverse datasets in time series forecasting benchmarks [21], can generalise to the volatility, negative-price regimes, and regime shifts characteristic of electricity markets. *Thirdly*, the majority of prior work reports performance only at an aggregated horizon-level. In multi-step forecasting settings, this typically involves averaging performance metrics across all forecast steps, which obscures how performance varies across individual intervals of the day. Electricity prices, however, exhibit a pronounced diurnal structure, with volatility, renewable output, and demand conditions varying across both daily and seasonal cycles. Intraday interval-level evaluation, for example, across all 48 half-hour intervals in 30-minute data, is therefore essential not only for understanding the difficulty of time-of-day forecasting, but also for diagnosing the true operational reliability of forecasting models. Such analysis is crucial for identifying model strengths and weaknesses during peak and off-peak periods, thereby enabling more targeted improvements and ensuring better alignment with real-world operational needs.

To address these gaps, this study proposes a novel DL-based EPF framework that systematically extends forecast horizons beyond the conventional day-ahead setting, thereby enabling multi-day-ahead forecasting. The framework integrates benchmarked SOTA time series DL models from general time series forecasting literature alongside standard DL models commonly adopted in EPF. The selected models span dominant DL families—including recurrent, convolutional, attention-based, and state-space architectures—and are incorporated within a unified experimental design for consistent evaluation across regions and horizons. The performance of the models is evaluated using standard magnitude- and direction-based metrics. Importantly, performance is also assessed separately for each of the 48 half-hour intervals of the day. This intraday interval-level analysis enables the identification of time-of-day forecasting challenges and provides insights into the underlying market and generation conditions that drive systematic error patterns.

In this paper, we focus on the Australian National Electricity Market (NEM), which spans five regions: Queensland (QLD), New South Wales (NSW) (including the Australian Capital Territory), Victoria (VIC), South Australia (SA), and Tasmania (TAS). The study utilises 30-minute aggregated data to forecast day-ahead (24-hour) and two-day-ahead (48-hour) periods, enabling multi-horizon forecasting. The use of a 30-minute resolution

is motivated by its suitability for medium-term operational decision-making (e.g., optimisation of BESS operation), for which 5-minute data are excessively granular and computationally burdensome over extended forecasting horizons.

Finally, unlike many recent EPF studies that combine DL models with signal decomposition techniques, this study explicitly excludes such preprocessing. While hybrid decomposition frameworks often yield improved performance, they confound the contribution of the forecasting architecture with that of the preprocessing strategy, making it difficult to disentangle the source of performance gains. By excluding decomposition, we isolate the intrinsic modelling capability of different DL architectures, allowing for a controlled and transparent comparison of model behaviour across regions, horizons, and diurnal intervals.

Therefore, this study makes several key contributions to the EPF literature, summarised as follows.

1. We extend the scope of the forecasting horizon in EPF from the conventional day-ahead forecasting to multi-day-ahead forecasting.
2. We address the gap in EPF by systematically adopting SOTA time series DL models, offering insights into how advances in time series forecasting benchmarks transfer to electricity price characteristics.
3. To the best of our knowledge, this is the first study to build and evaluate forecasting models across all five regions of the NEM, enabling a rigorous assessment of model generalisability and revealing how performance varies across regions.
4. We introduce a granular, intraday half-hourly performance analysis, uncovering systematic time-of-day error patterns that are otherwise obscured by conventional aggregated horizon-level evaluation.

The remainder of this paper is organised as follows. Section 2 reviews the relevant literature on DL-based EPF and summarises recent SOTA advancements in general-purpose time series forecasting. Section 3 describes the methodology, including the datasets, models, training procedures, and evaluation. Section 4 presents and analyses the results, offering a detailed discussion of model performance across regions, horizons, and diurnal intervals. Section 5 concludes the paper by summarising the key findings and outlining directions for future research.

2. Related Work

2.1. Electricity Price Forecasting with Deep Learning

EPF has been extensively studied across various forecasting approaches, with recent developments increasingly centered on DL. Accordingly, this section reviews recent DL-based EPF studies. In particular, the literature is analysed with respect to the temporal granularity of price data, the forecasting horizons considered, and the evolution of modelling architectures and associated enhancements employed across different electricity markets. This focused review provides context for the methodological design of this study.

Existing EPF studies exhibit substantial variation in data granularity. Hourly electricity price data constitutes the dominant data resolution in forecasting studies across a wide range of markets, including the European Power Exchange (EPEX) [22] and the Nord Pool electricity market [23, 24], as well as North American market systems operated by the PJM Interconnection LLC (PJM) [25] and the New York Independent System Operator (NYISO) [26]. Hourly data are also widely used in other international markets, including Iran [27] and China [28]. A subset of studies adopts finer temporal resolutions to better capture intraday price dynamics, particularly in markets characterised by higher volatility and increasing renewable penetration. These include half-hourly price data in Australian regions such as NSW [29], QLD [30], and VIC [31], 15-minute resolution data in markets operated by the European Network of Transmission System Operators for Electricity (ENTSO-E) [32], and 5-minute price series in the Ontario electricity market [33]. Despite this variation in data resolution, the forecasting scope remains consistently focused on short-term horizons. Existing studies primarily consider hour-ahead prediction tasks [34, 35], in some cases extending to 2–3 hours ahead [36], as well as day-ahead forecasting configurations [37, 38, 39]. These horizons support applications ranging from real-time operational scheduling to short-term strategic planning. To better adapt to volatile market conditions, several studies employ rolling-horizon forecasting frameworks, which repeatedly update predictions as new information becomes available [40, 41].

Methodologically, recent EPF research reflects diverse modelling strategies aimed at capturing nonlinear and time-dependent behaviour in electricity prices. Early work applied an Artificial Neural Network in EPEX [22] and a Deep Neural Network in the Belgian market [37], establishing the feasibility of data-driven nonlinear mappings for day-ahead forecasting. Subsequent stud-

ies increasingly adopted sequence models, most notably Long Short-Term Memory (LSTM) networks in markets such as Nord Pool [23]. In parallel, wavelet decomposition was integrated with LSTM for hour- and day-ahead forecasting in NSW and France [42]. More recently, Iwabuchi et al. [43] addressed the limitation of fixed wavelet decomposition in wavelet–LSTM electricity price forecasting models by periodically switching the mother wavelet to adapt to changing daily and seasonal time series characteristics. Decomposition-enhanced variants were explored in approaches such as Maximal Overlap Discrete Wavelet Transform–Empirical Mode Decomposition–LSTM [24]. Related work has also introduced Gated Recurrent Unit (GRU)-based formulations and hybrids, including Variational Mode Decomposition–Convolutional Neural Network (CNN)–GRU in NYISO [26] and GRU–Light Gradient Boosting Machine model in China [28]. Convolutional–recurrent combinations are similarly prominent, including CNN–LSTM architectures in PJM [25] and Iran [27], as well as CNN–Bidirectional LSTM (BiLSTM)–Autoregressive model in the United Kingdom and Germany [39]. More recent contributions incorporate structured attention and spatial learning, including one-dimensional CNN with self-attention model in Ontario [44], tri-head parallel CNN–GRU architectures for short-term forecasting in Ontario [36], and Graph Convolutional Network (GCN) models with attention mechanisms in PJM [45]. Transformer-based architectures have also emerged, including a Transformer–BiLSTM model in NYISO [34] and a hybrid spatio-temporal framework that combines GCN–Transformer components in ENTSO-E settings [32], reflecting a growing interest in attention-driven representations for short-term EPF.

In summary, the existing literature demonstrates a strong concentration on short-term EPF using hourly and sub-hourly data, with forecasting horizons largely confined to hour-ahead and day-ahead settings. Architecturally, research has progressed from early feedforward neural networks toward recurrent, convolutional, and attention-based architectures, with hybridisation often incorporating decomposition.

2.2. Recent Advancements in Time Series Forecasting

Time series forecasting has undergone rapid architectural evolution in recent years. The development of contemporary forecasting models reflects a shift from sequential dependency modelling to architectures that emphasise the decomposition of intrinsic time series properties, such as trend, seasonality, and periodicity, along with variations in attention mechanisms. These

advances aim to capture nonlinear and long-range temporal dependencies as well as cross-variable relationships while enhancing interpretability and computational efficiency. A core innovation across many of these new architectures has been the reduction of the computational complexity from the quadratic $O(L^2)$ of the original Transformer to linear or near-linear scaling, a critical factor for handling the long input sequences often required for long-term forecasting.

Table 1 summarises representative time series forecasting models developed in recent years, categorised by their architectural families. These include Multilayer Perceptron (MLP), CNN, Transformer-based, and State-Space Model (SSM)-based models. Notably, these models have demonstrated SOTA performance on popular time series benchmark datasets, including ETT (Electricity Transformer Temperature), Weather, Exchange Rate, and ILI (Influenza-Like Illness). However, these benchmark datasets are relatively smooth and stationary compared to the high-volatility dynamics of electricity prices. Therefore, it remains an open question whether these models can maintain their efficiency and accuracy when applied to complex non-stationary time series such as electricity prices. Given these challenges, it is crucial to investigate whether recent advances in general-purpose time series forecasting can be effectively applied to EPF. With this motivation, the following section discusses the key innovations underlying these models.

Table 1: Recently proposed time series forecasting models and their key innovations.

Model	Year	Family	Key Idea
N-BEATS [46]	2020	MLP	Residual MLP blocks; learnable basis for trend and seasonality.
Former [47]	2021	Transformer	ProbSparse self-attention; attention distillation for long sequences.
Autoformer [48]	2021	Transformer	Auto-correlation attention; built-in trend-seasonal decomposition.
SCINet [49]	2022	CNN	Recursive block decomposition; inter-series interaction.
S4 [50]	2022	SSM	Structured state-space layers for long-range dependencies; linear-time complexity.
FEDformer [51]	2022	Transformer	Fourier transform-based attention; efficient long-range modelling.
PatchTST [52]	2023	Transformer	Patch tokenization; channel-independent attention mechanism.
DLinear [53]	2023	MLP	Linear trend-seasonal decomposition with moving averages.
TimesNet [54]	2023	CNN	Converts 1D series to 2D temporal tensors to capture multi-period patterns.
iTransformer [55]	2023	Transformer	Variate-centric tokens; attention operates across variables.
Mamba [56]	2024	SSM	Selective state-space layers enabling efficient long-sequence modeling.
TimeMixer [57]	2024	MLP	Past-Decomposable Mixing and Future-Multipredictor-Mixing.
TimeXer [58]	2024	Transformer	Patch attention with cross-variable fusion for exogenous inputs.

2.2.1. MLP-based models

A major trend in recent research has been the explicit separation of temporal components through decomposition-based and MLP architectures, em-

phasising interpretability and efficiency. The N-BEATS [46] model introduced a residual MLP architecture that learns basis functions for trend and seasonality, achieving high accuracy while remaining interpretable. This design enabled competitive forecasting performance without reliance on complex architectures, demonstrating the continued relevance of simple models. Building on this principle, DLinear [53] applied a lightweight linear decomposition using moving averages, providing a strong baseline that often rivals transformer models in accuracy but at a fraction of their computational cost. The more recent TimeMixer [57] model combined multi-scale decomposition with specialised modules: the Past-Decomposable Mixing module and Future-Multipredictor-Mixing module. The Past-Decomposable Mixing module includes specific Trend Mixing and Seasonal Mixing components to process the respective historical time series components, and the Future-Multipredictor-Mixing module is responsible for generating accurate forecasts. These two modules together enable the simultaneous modelling of temporal patterns and cross-variable dependencies efficiently.

2.2.2. Transformer-based Models

In parallel with MLP-based models, transformer-based architectures have fundamentally revolutionised time series forecasting by enabling global context modelling through self-attention mechanisms. The transformer’s ability to learn pairwise dependencies across all time steps has proven highly effective for capturing long-range temporal interactions. Yet, the quadratic complexity of vanilla attention posed computational challenges for long sequences, leading to numerous innovations. Informer [47] introduced Prob-Sparse attention and attention distillation to efficiently scale transformers to long sequences. Autoformer [48] incorporated trend-seasonal decomposition directly into its attention layers, enhancing interpretability and stability for long-horizon forecasts. FEDformer [51] moved this concept into the frequency domain, using Fourier-based attention to capture periodic patterns while improving computational efficiency. More recent models, such as PatchTST [52], inspired by Vision Transformers, tokenise continuous time series into fixed-length patches to better model local patterns. Whereas iTransformer [55] inverts the attention direction to focus on variable-level interactions instead of time, thereby improving performance in multivariate forecasting tasks. Meanwhile, TimeXer [58] integrates structured patch attention mechanisms with a cross-variable fusion module to explicitly leverage exogenous inputs.

2.2.3. SSM and CNN-based Models

The SSM family offers a compelling alternative to Transformers, designed specifically for efficient modelling of continuous and long-range dependencies, with linear complexity. S4 (Structured State Space Model) [50] provided the theoretical and computational foundation, demonstrating how continuous-system dynamics can be efficiently discretised and utilised in DL for long-sequence tasks. Mamba [56] is the current SOTA within this family, introducing a Selective State Space layer. This key innovation enables the model’s recurrent state to be dynamically filtered based on the input, effectively providing it with an attention-like mechanism for focusing on relevant information while maintaining linear-time complexity and parallelised training. Recently, Mamba has gained significant attention and adoption in time series forecasting [59], where it has achieved leading performance with lower computational overhead compared to Transformer-based models.

In contrast, CNN-based models such as SCINet [49] and TimesNet [54] excel at learning localised temporal patterns through hierarchical convolutional structures, efficiently capturing the multi-periodic behavior in time series. SCINet introduced recursive downsampling and convolution to capture multi-resolution temporal features. TimesNet achieved significant breakthroughs by converting 1D time series data into 2D tensors based on multiple inferred periods. This transformation, based on the assumption that the signal is driven by a few dominant periodic components, allows 2D CNN kernels to simultaneously capture complex, hidden multi-period patterns.

3. Methodology

We propose a novel DL-based EPF framework, illustrated in Figure 1, designed to systematically extend forecasting horizons beyond the conventional day-ahead setting. The framework integrates recent NEM price data, standardised data preparation procedures, and a diverse set of forecasting models, including both standard DL models commonly used in EPF and benchmarked SOTA time series DL models from the general time series forecasting literature. It also applies a comprehensive hyperparameter optimisation strategy to ensure consistent and fair model evaluation. The full workflow from data acquisition to model evaluation is described in the following subsections.

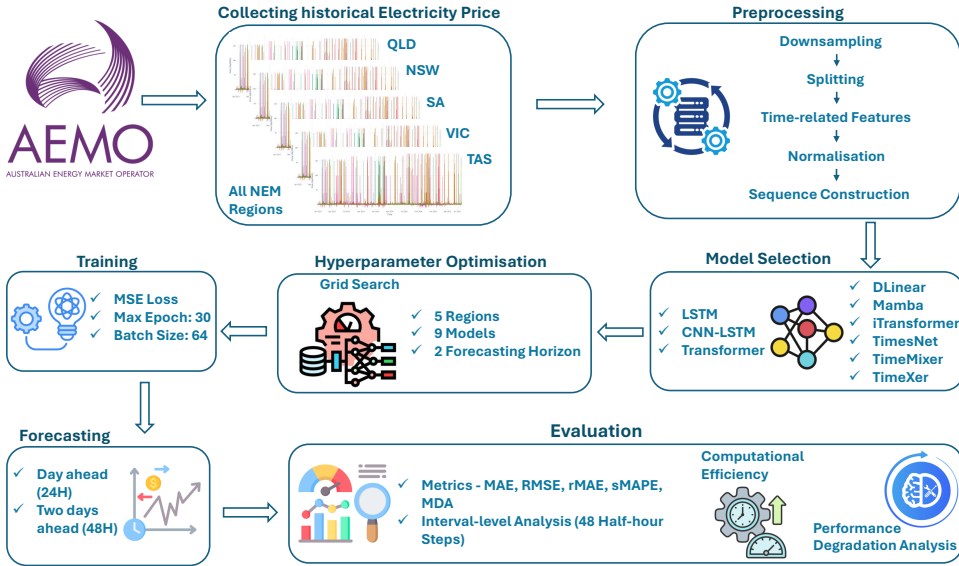


Figure 1: An overview of the proposed EPF framework in this study, encompassing the stages of NEM data acquisition through data preparation, model selection, hyperparameter optimisation, training to forecasting, and performance evaluation.

3.1. Datasets

For a comprehensive evaluation, we use wholesale electricity price data from all five regions of the NEM in Australia: QLD, NSW (includes the Australian Capital Territory), VIC, SA, and TAS. The data correspond to the Regional Reference Price (RRP), which represents the spot market clearing price in each region. We retrieved the data from the Australian Energy Market Operator (AEMO)¹ using the `nemdatatools` Python library². The dataset covers the period from January 1, 2023, to June 30, 2025, with a 5-minute temporal resolution (262,656 observations per region), reported in Australian Eastern Standard Time under the current 5-minute settlement regime³. Zero, negative, and extreme price observations are retained to preserve genuine market dynamics, and no smoothing or filtering is applied.

¹<https://www.aemo.com.au/>

²<https://pypi.org/project/nemdatatools/>

³<https://www.aemo.com.au/initiatives/major-programs/past-major-programs/five-minute-settlement>

A key reason for selecting this period is that it reflects the most recent operational and structural conditions of the NEM. This time window captures the post-COVID market environment, where demand patterns have stabilised following pandemic-related disruptions. It also coincides with a rapid increase in variable renewable energy (VRE) penetration, particularly solar and wind, which has fundamentally reshaped intraday price formation and contributed to negative prices, steeper ramps, and higher short-term volatility⁴ ⁵. Finally, the 5-minute settlement rule, fully implemented in late 2021, was well established during this period, ensuring that the data represent the current dispatch and pricing structure. Using recent data, therefore, enables the models to be evaluated under contemporary market dynamics rather than historical conditions that may no longer be representative.

3.2. Data Preparation

Downsampling. AEMO operates under a 5-minute settlement framework, with both dispatch and spot prices determined at 5-minute intervals. For the purposes of this study, the price series were converted to a 30-minute resolution to align with the temporal scale of medium-term operational analysis and to ensure computational tractability for multi-step forecasting. Specifically, the original 5-minute Regional Reference Price (RRP) data were down-sampled by computing the arithmetic mean of six consecutive observations to form each 30-minute value. This transformation was applied consistently across all five NEM regions, reducing the number of observations from 262,656 to 43,776 per regional dataset. As the original data contained no missing timestamps or missing values, no imputation was required.

Data Splitting. The datasets are chronologically divided into training, validation, and testing subsets. Data from January 1, 2023, to December 31, 2024, are used for model training and validation, with 70% allocated to training and the remaining 30% for validation. The most recent six-month period, from January 1, 2025, to June 30, 2025, is held out for testing and inference. This forward-looking temporal split ensures that future information is not leaked into the training process, thereby providing a realistic evaluation

⁴<https://www.aemo.com.au/energy-systems/major-publications/quarterly-energy-dynamics-qed>

⁵<https://www.energycouncil.com.au/analysis/renewables-in-the-nem-are-they-leading-to-price-extremes/>

of the model’s forecasting capability. Figure 2 illustrates the chronological division applied to the QLD region dataset as an example.

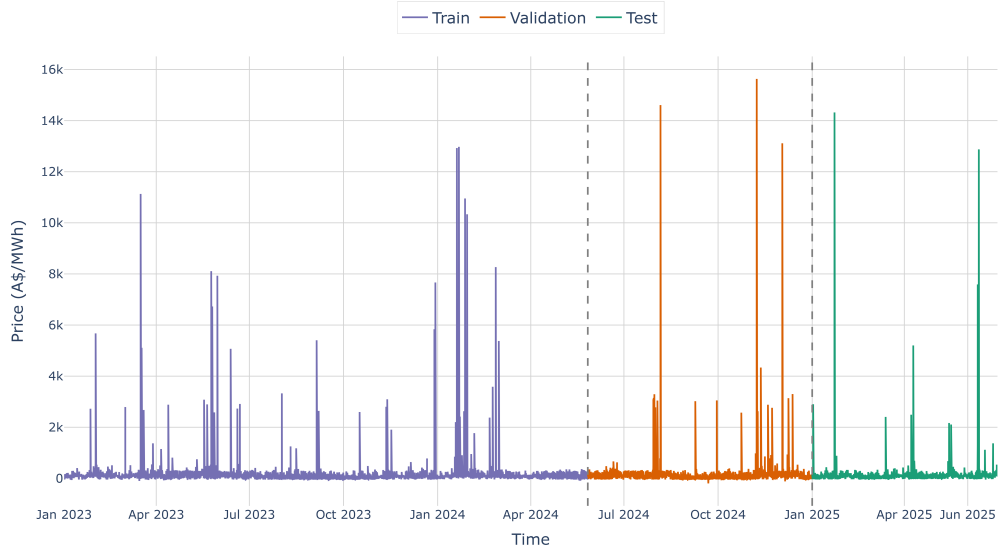


Figure 2: Train, validation, and test splits of the electricity price data for the QLD region.

Time-related Features. The SOTA time series forecasting models evaluated in this study require time-related features as part of their input representations. Accordingly, four temporal features were extracted from the timestamps. These include:

- Hour of day (1–24),
- Day of week (1–7),
- Day of month (1–31), and
- Month of year (1–12).

These features are incorporated only into the SOTA time series models, as they are integral to the design of these architectures.

Normalisation. Prior to model training, all input features are normalised using the Min–Max scaling method to the range $[0, 1]$. Normalisation ensures that all variables contribute equally to model training, preventing features with larger numerical ranges from dominating the optimisation process. Moreover, Min–Max normalisation facilitates faster convergence in gradient-based models and helps maintain numerical stability during training. This approach is widely adopted in recent EPF studies. The normalisation is applied as follows:

$$x_{\text{norm}} = \frac{x - x_{\text{min}}}{x_{\text{max}} - x_{\text{min}}} \quad (1)$$

where x denotes the original feature value, and x_{min} and x_{max} are the minimum and maximum values observed in the training dataset, respectively.

Sequence Construction. The normalised price series are transformed into input–output sequences for two experimental settings:

1. A 7-day lookback window (336 half-hourly observations) used to forecast the next 24 hours (48 steps), representing the day-ahead forecasting task.
2. A 14-day lookback window (672 half-hourly observations) used to forecast the next 48 hours (96 steps), representing the two-day-ahead forecasting task.

All models follow a direct multi-step forecasting strategy, where a single forward pass predicts the full 48-step forecast for the 24-hour horizon and the 96-step forecast for the 48-hour horizon.

3.3. Model Selection

Within the proposed DL-based EPF framework, the model section strategy was designed to cover existing baseline DL models in EPF and also more recent, general-purpose SOTA time series DL models. This enables us to evaluate whether recent methodological advances in time series forecasting are effectively transferable to the EPF domain. Below, we describe the model selection strategy and the rationale behind it.

Models from Existing EPF Research. The comprehensive review of existing EPF studies in Section 2.1 revealed that among recurrent models, LSTM and GRU are the widely applied, with LSTM being the most frequently used. Accordingly, we selected LSTM as the representative recurrent model for this

study. Although GRU is often preferred for its lower computational cost, computational efficiency is not the primary focus of our analysis. Hybrid DL models that combine convolutional and recurrent structures—particularly CNN-LSTM—are also widely applied in the EPF literature; therefore, we included CNN-LSTM as a representative hybrid architecture. In addition, recent EPF studies have increasingly utilised transformer-based architectures, motivated by their ability to model long-term dependencies via self-attention mechanisms. For this reason, the Transformer model was also incorporated into our framework. Together, LSTM, CNN-LSTM, and Transformer represent the dominant DL model families explored in existing EPF research covering recurrent, hybrid, and attention-based models. However, a noted challenge in the EPF field is the limited reproducibility of existing publications. Given that exact replication of prior implementations was not feasible, we constructed our own representative implementations of these architectures.

Models from Recent Time Series Forecasting Research. We reviewed SOTA DL models from the general time series forecasting literature (see Section 2.2). Numerous models have been proposed in recent years; a subset of the most influential ones is summarised in Table 1, categorised according to their underlying algorithmic family. Following the benchmarking leaderboard⁶ that ranks recent long-term forecasting models, we selected two top-performing models, TimeXer and TimeMixer, representing the lookback-searching and lookback-96 subcategories, respectively. Furthermore, to ensure coverage across major model families, we selected one representative model from each: DLinear from the MLP family, TimesNet from the CNN family, iTransformer from the Transformer family, and Mamba from the SSM family.

Selected Models. In total, we adopted six benchmarked SOTA time series DL models alongside three standard DL models commonly used in existing EPF research. The detailed mathematical formulations of these models are skipped in this article for brevity; we refer the reader to the original articles (DLinear [53], TimesNet [54], iTransformer [55], Mamba [56], TimeMixer [57], TimeXer [58]) for their comprehensive technical descriptions.

⁶<https://github.com/thuml/Time-Series-Library>

3.4. Hyperparameter Optimisation

We conducted a comprehensive hyperparameter search for all models using the grid search method to ensure fairness in performance comparison (see Table 2). The hyperparameter search was performed across datasets from five different regions and for two forecasting horizon settings. This resulted in a total of 2 experiment settings \times 5 datasets = 10 unique searches for each of the 9 models. For the LSTM, Mamba, Transformer, iTransformer, TimesNet, TimeMixer, and TimeExer models, the dimensions of the model (i.e., hidden units), the number of layers, and the learning rate (LR) were optimised, resulting in 50 combinations in one search. DLinear has only one tunable hyperparameter, the LR, while for CNN-LSTM, the number of filters in the CNN, filter size, LSTM hidden dimension, and LR were optimised, leading to 375 combinations in one search.

Table 2: Hyperparameter Search Space (LR: Learning Rate; Dim: Hidden Dimensions; N. Layers: Number of Layers; F. Size: Filter Size; Filters: Number of Filters).

Model(s)	LR	Dim.	N. Layers	F. Size	Filters
LSTM, Mamba, Transformer, iTransformer, TimesNet, TimeMixer, TimeExer	0.001–0.1 ^a	32–512 ^b	1–2	N/A	N/A
DLinear	0.001–0.1 ^a	N/A	N/A	N/A	N/A
CNN-LSTM	0.001–0.1 ^a	32–512 ^{b,*}	N/A	3–7 ^c	32–512 ^b

^a 0.001, 0.005, 0.01, 0.05, 0.1.

^b 32, 64, 128, 256, 512.

^c 3, 5, 7.

* LSTM Hidden Dimension.

The search space for hidden units was selected based on ranges commonly used in existing time series forecasting models, with a maximum hidden dimension of 512 . Specifically, the number of hidden units was searched in powers of 2 between 32 and 512 , the CNN filter sizes between 3 and 7 , and the number of hidden layers between 1 and 2 . For the LR, we followed the ranges typically used in SOTA time series models, which are between 0.001 and 0.05 . However, our preliminary search indicated that the optimal LR for many models was 0.05 . Consequently, we expanded the search space to include a larger value of 0.1 . It is worth noting that the values defined in the search space were used as the initial rates, which were subsequently adjusted

through an LR scheduler. The hyperparameter search space for all models is presented in Table 2. The resulting optimal hyperparameters are provided in the Appendix (see Table A.1 - Table A.5).

3.5. Experimental Setup

We conducted all experiments in Python, primarily utilising the PyTorch framework. For the SOTA time series models, we collected the original source code from the authors' official GitHub repositories. For hyperparameter tuning and the final training runs, all code was executed on NVIDIA H100 Tensor Core GPUs (80GB VRAM), within a resource allocation limit of 256 GB of system memory and 12 CPU cores.

Training for all models was optimised using the Adam optimiser, with the Mean Squared Error (MSE) as the loss function. We employed an LR scheduler, ReduceLROnPlateau (with patience = 3 and factor = 0.5), to adjust the rate dynamically during training. Models were trained for a maximum of 30 epochs with a batch size of 64, and we utilised an early stopping mechanism with a patience of 10 epochs based on the validation loss. For the reported results, we conducted each experiment five (5) times using different random seeds, ensuring a robust and fair comparison of the models. The source code for these experiments is publicly available in GitHub⁷.

3.6. Evaluation

The evaluation criteria in this study are structured around three dimensions. First, we assess forecasting accuracy using a set of standard error- and direction-based metrics. These accuracy measures are evaluated both in aggregated form and at the interval level across the 48 half-hour intervals of the day, enabling a diurnal assessment of time-of-day-dependent forecasting behaviour. Second, we examine horizon sensitivity by quantifying performance degradation when extending the forecast window from 24 hours to 48 hours, providing insight into the robustness of each model under longer-term prediction requirements. Third, we assess the computational efficiency of each model, using total training time and the average time per epoch, to offer practical context regarding the resource demands of each modelling approach. Collectively, these components form a comprehensive framework for evaluating the EPF models.

⁷<https://github.com/GaniMosman/Multi-Horizon-EPF-NEM.git>

3.6.1. Metrics

We evaluate the performance of the day-ahead and two-day-ahead price forecasts using five performance metrics. Four of these, Mean Absolute Error (MAE), Root Mean Square Error (RMSE), Relative Mean Absolute Error (rMAE), and Symmetric Mean Absolute Percentage Error (sMAPE), quantify magnitude-based forecasting errors, where rMAE explicitly evaluates model performance relative to a benchmark forecast. These metrics measure how closely the predicted prices \hat{y}_t align with the actual observed prices y_t . The fifth metric, Mean Directional Accuracy (MDA), assesses whether the model correctly predicts the direction (trend) of price movements, capturing the model's ability to anticipate whether prices will rise or fall. Together, these metrics evaluate both the magnitude and direction of forecasting deviations, providing a comprehensive evaluation of models widely used in electricity price [60] and time series forecasting [61].

MAE. MAE measures the average magnitude of forecast errors in the same unit as the electricity price (AU\$/MWh), providing an interpretable indication of typical deviation from the actual prices without considering their direction. It is defined as:

$$\text{MAE} = \frac{1}{N} \sum_{i=1}^N |y_i - \hat{y}_i| \quad (2)$$

where N is the total number of forecast points. For EPF, a lower MAE indicates that the model can effectively track general market dynamics. This is due to MAE's linear penalty, where the error contribution is directly proportional to the size of the deviation. Crucially, this means MAE does not heavily penalise large price spikes in a disproportionate fashion, making it less sensitive to outliers compared to squared-error-based measures.

RMSE. RMSE quantifies the square root of the average squared differences between actual and predicted values. It penalises large deviations quadratically due to the squaring operation, making it sensitive to extreme deviations. Similar to MAE, it is expressed in the original data units, allowing comparison with the raw price values. RMSE can be defined as:

$$\text{RMSE} = \sqrt{\frac{1}{N} \sum_{i=1}^N (y_i - \hat{y}_i)^2} \quad (3)$$

In electricity markets, where usually extreme price spikes occur, RMSE provides insight into the model’s ability to handle such outlier events. A lower RMSE implies that the model can not only follow average price trends but also mitigate large forecasting errors.

rMAE. rMAE is a scale-independent metric designed to evaluate a model’s performance relative to a defined benchmark, commonly a seasonal naïve forecast. It is calculated as the ratio of the MAE of the forecasting model to the MAE of the benchmark model on the same out-of-sample data. This effectively measures the magnitude of the model’s error relative to that of the benchmark. rMAE is defined as:

$$\text{rMAE} = \frac{\text{MAE}_{\text{model}}}{\text{MAE}_{\text{benchmark}}} = \frac{\frac{1}{N} \sum_{i=1}^N |y_i - \hat{y}_i|}{\frac{1}{M-f} \sum_{t=f+1}^M |y_t - y_{t-f}|} \quad (4)$$

where the denominator represents the MAE of the seasonal naïve benchmark. This benchmark is calculated using the out-of-sample series, y_t , and its forecast, y_{t-f} , which is simply the observed value from f periods ago. The variable f denotes the seasonal frequency of the data. In this study, a weekly seasonal naïve forecast is employed ($f = 336$ for 30-minute interval data), as recommended by [62]. Accordingly, y_{t-f} corresponds to the price observed exactly one week earlier.

rMAE values are interpreted as follows:

- $\text{rMAE} < 1$: The model outperforms the weekly seasonal naïve benchmark.
- $\text{rMAE} = 1$: The model performs similarly to the naïve forecast.
- $\text{rMAE} > 1$: The model performs worse than the benchmark.

sMAPE. Measuring forecast error as a percentage of the actual value is valuable because it enables scale-independent comparison across diverse datasets, such as different electricity markets. It also provides an intuitive interpretation of the relative magnitude of errors in relation to the true values. However, the calculation of a standard proportional percentage error, such as the Mean Absolute Percentage Error (MAPE), presents notable drawbacks. In EPF, actual values (y_i) can frequently be zero or very close to zero, causing MAPE, which uses y_i in the denominator, to become unstable, undefined, or biased towards overestimation.

To overcome the above issues, sMAPE is employed, which quantifies forecast accuracy as a percentage, remaining robust even when actual values are small or zero. It is defined as:

$$\text{sMAPE} = \frac{100}{N} \sum_{i=1}^N \frac{|y_i - \hat{y}_i|}{(|y_i| + |\hat{y}_i|) / 2} \quad (5)$$

By normalising with the average of the actual and predicted values, sMAPE avoids division by zero and provides a balanced assessment of over- and under-forecast errors. However, a practical limitation may still arise in EPF: when the actual value (y_i) and the predicted value (\hat{y}_i) have opposite signs (e.g., an actual negative price and a predicted positive price), the denominator can approach zero. In such situations, sMAPE can still become unstable and exceed its theoretical bounds between 0% and 200%.

MDA. Beyond magnitude-based accuracy, predicting the direction of price movements is valuable for a range of operational and trading decisions. MDA, expressed as a percentage for interpretability, measures how often the forecasted trend correctly anticipates the direction of price changes over consecutive time steps. For multi-step forecasts, MDA is defined as:

$$\text{MDA} = \frac{1}{N-1} \sum_{t=2}^N \mathbf{1}[\text{sign}(\hat{y}_t - \hat{y}_{t-1}) = \text{sign}(y_t - y_{t-1})] \times 100 \quad (6)$$

where $\mathbf{1}[\cdot]$ is an indicator function equal to 1 if the predicted change direction matches the actual change direction, and 0 otherwise.

MDA can be interpreted as:

- MDA = 100%: Model perfectly predicts the direction of price changes.
- MDA = 50%: Directional accuracy is at chance level.
- MDA < 50%: Model performs worse than random in predicting direction.

3.6.2. Performance Degradation Calculation

To quantify the change in model performance when extending the forecast horizon, we compute a degradation percentage ($\Delta\%$) for each evaluation

metric. Let H_1 and H_2 denote the two forecast horizons. For error-based metrics (MAE, RMSE, sMAPE, and rMAE), the degradation is defined as:

$$\Delta\% = \frac{V_{H_2} - V_{H_1}}{V_{H_1}} \times 100\%, \quad (7)$$

where V_{H_1} and V_{H_2} represent the metric values at the 24-hour and 48-hour forecasting horizons, respectively.

For MDA, where higher values indicate better performance, the degradation is computed as:

$$\Delta\% = \frac{V_{H_1} - V_{H_2}}{V_{H_1}} \times 100\%. \quad (8)$$

This formulation ensures a consistent interpretation across all metrics: a positive $\Delta\%$ indicates performance degradation when extending to the two-day-ahead horizon, while a negative $\Delta\%$ indicates performance improvement.

4. Results and Discussion

4.1. Model Performance

4.1.1. Region-based Performance Analysis

Tables 3-7 present a comprehensive comparison of model performance across all five NEM regions for both 24-hour and 48-hour forecast horizons. These results enable us to examine how various forecasting models behave under the diverse price dynamics present in each market. Although the tables provide detailed metric values, several overarching patterns emerge that help contextualise the relative behaviour of the models.

For the 24-hour horizon, the standard DL models consistently appear as either the best or second-best across most regions. In QLD, NSW, SA, and TAS, at least two of these three models dominate the top positions. In several regions, particularly NSW and SA, CNN-LSTM often secures the best overall results, with LSTM or Transformer following closely as the second-best. This suggests that recurrent temporal modelling combined with convolutional feature extraction remains highly effective for electricity price dynamics in these markets, outperforming SOTA time series models. Standard Transformer models also outperform the rest of the models in the QLD market, performing competitively and frequently ranking among the top two, particularly in terms of RMSE and MDA. In VIC, the SOTA time series dominates; together, they ranked first in all metrics and also second-best in most cases.

Table 3: Models Performance on the **QLD** Dataset Across 24-Hour and 48-Hour Forecast Horizons.

Model	24H					48H				
	MAE	RMSE	sMAPE	rMAE	MDA	MAE	RMSE	sMAPE	rMAE	MDA
CNN-LSTM	59.031	393.466	57.575	0.744	66.184	<u>64.178</u>	407.157	62.298	0.808	65.574
DLinear	77.637	408.145	68.122	0.978	54.644	91.225	424.292	78.473	1.149	54.039
LSTM	<u>57.875</u>	393.397	56.145	<u>0.729</u>	<u>65.358</u>	<u>64.477</u>	<u>408.129</u>	<u>65.535</u>	<u>0.812</u>	64.684
Mamba	58.696	<u>392.834</u>	<u>57.027</u>	0.739	62.951	71.461	425.951	65.652	0.9	63.5
TimeMixer	88.805	498.688	64.259	1.119	59.862	89.398	429.763	71.812	1.126	57.093
TimeXer	65.849	396.833	61.959	0.829	59.778	76.23	418.272	68.122	0.96	59.865
TimesNet	75.25	490.291	63.128	0.948	63.298	83.498	472.201	70.736	1.052	63.184
Transformer	54.938	386.188	57.542	0.692	64.536	64.802	410.117	65.7	0.816	<u>65.010</u>
iTransformer	75.475	443.239	63.822	0.951	59.033	76.922	422.678	69.505	0.969	60.505

Note: Lower values indicate better performance, except for MDA, where higher values are preferred. MAE and RMSE are reported in Australian dollars (A\$/MWh). Best and second-best results are indicated in **bold** and underline, respectively.

Table 4: Models Performance on the **NSW** Dataset Across 24-Hour and 48-Hour Forecast Horizons.

Model	24H					48H				
	MAE	RMSE	sMAPE	rMAE	MDA	MAE	RMSE	sMAPE	rMAE	MDA
CNN-LSTM	82.409	513.079	56.104	0.798	61.397	96.16	584.364	61.991	0.931	62.851
DLinear	102.954	515.743	66.8	0.997	53.817	98.861	<u>518.314</u>	67.805	0.958	53.97
LSTM	86.414	511.609	<u>61.144</u>	0.837	59.831	89.618	524.464	<u>61.814</u>	0.868	<u>61.924</u>
Mamba	<u>82.448</u>	518.251	61.385	<u>0.799</u>	58.667	85.856	519.28	62.827	0.832	61.315
TimeMixer	98.054	514.872	71.03	0.95	52.922	93.128	518.969	70.144	0.902	52.161
TimeXer	89.044	519.295	63.446	0.862	57.533	93.506	519.353	73.65	0.906	54.895
TimesNet	91.024	523.729	63.26	0.882	57.243	91.464	518.829	69.97	0.886	55.384
Transformer	84.095	<u>511.923</u>	62.983	0.815	<u>60.939</u>	<u>89.388</u>	517.518	61.015	<u>0.866</u>	60.921
iTransformer	89.408	517.652	66.079	0.866	57.073	89.951	520.873	66.305	0.871	57.336

Note: Lower values indicate better performance, except for MDA, where higher values are preferred. MAE and RMSE are reported in Australian dollars (A\$/MWh). Best and second-best results are indicated in **bold** and underline, respectively.

When the forecasting horizon is extended to 48 hours, performance becomes more nuanced. While the standard DL baselines still perform strongly in many regions, newer SOTA time series models begin to outperform them in several cases. For example, TimeXer achieves the best or second-best performance in SA, TAS, and VIC, while Mamba shows competitive performance in NSW and SA. However, the LSTM and CNN-LSTM models still maintain the best or second-best performance in multiple regions, such as QLD and TAS, indicating that their capabilities remain robust even as the

Table 5: Models Performance on the **SA** Dataset Across 24-Hour and 48-Hour Forecast Horizons.

Model	24H					48H				
	MAE	RMSE	sMAPE	rMAE	MDA	MAE	RMSE	sMAPE	rMAE	MDA
CNN-LSTM	87.158	490.976	86.692	0.708	62.358	100.908	509.015	96.704	0.819	57.832
DLinear	95.607	<u>487.599</u>	89.818	0.776	53.947	99.231	499.648	93.248	0.806	54.741
LSTM	<u>88.321</u>	491.239	88.504	<u>0.717</u>	<u>59.626</u>	99.872	509.8	96.72	0.811	56.831
Mamba	89.231	494.933	88.258	0.725	59.555	<u>96.045</u>	505.923	92.239	<u>0.780</u>	59.743
TimeMixer	96.21	490.463	88.494	0.781	57.432	103.727	504.528	94.523	0.842	54.135
TimeXer	90.984	484.042	<u>87.400</u>	0.739	59.055	93.963	<u>499.855</u>	90.905	0.763	56.253
TimesNet	96.504	489.439	93.473	0.784	57.928	98.355	501.358	95.296	0.799	<u>58.782</u>
Transformer	90.798	492.023	87.686	0.737	59.328	100.309	507.358	94.51	0.815	57.601
iTransformer	95.388	487.948	91.298	0.775	57.122	101.108	502.003	95.966	0.821	58.371

Note: Lower values indicate better performance, except for MDA, where higher values are preferred. MAE and RMSE are reported in Australian dollars (A\$/MWh). Best and second-best results are indicated in **bold** and underline, respectively.

Table 6: Models Performance on the **TAS** Dataset Across 24-Hour and 48-Hour Forecast Horizons.

Model	24H					48H				
	MAE	RMSE	sMAPE	rMAE	MDA	MAE	RMSE	sMAPE	rMAE	MDA
CNN-LSTM	46.562	296.75	<u>36.543</u>	0.7	54.578	51.614	306.289	40.205	0.776	53.78
DLinear	53.765	296.015	42.538	0.809	51.334	57.997	306.038	46.357	0.872	51.179
LSTM	<u>46.443</u>	297.064	37.046	<u>0.699</u>	56.297	<u>51.324</u>	<u>305.927</u>	<u>40.066</u>	<u>0.772</u>	54.775
Mamba	46.071	297.836	36.565	0.693	54.546	53.569	308.344	41.715	0.806	<u>54.737</u>
TimeMixer	50.24	297.451	38.292	0.756	55.251	57.334	309.074	42.89	0.862	52.144
TimeXer	46.783	<u>296.559</u>	36.246	0.704	54.503	49.459	305.054	39.140	0.744	53.362
TimesNet	48.768	299.065	37.449	0.733	55.283	52.82	307.377	41.715	0.794	53.646
Transformer	48.263	299.326	37.361	0.726	53.675	51.753	306.654	40.234	0.778	52.913
iTransformer	51.438	298.873	38.549	0.774	<u>55.288</u>	53.886	307.291	42.175	0.81	50.0

Note: Lower values indicate better performance, except for MDA, where higher values are preferred. MAE and RMSE are reported in Australian dollars (A\$/MWh). Best and second-best results are indicated in **bold** and underline, respectively.

forecasting window extends.

An analysis of the rMAE provides further insights by benchmarking their performance against a simple weekly naïve model. Across both the 24-hour and 48-hour horizons, the standard DL models (LSTM, CNN-LSTM, and Transformer) consistently achieve an rMAE below 1 in all regions, indicating that they outperform the weekly naïve model universally. The SOTA time series models also achieve an rMAE below 1 in four out of the five regions for both horizons. However, a notable exception is observed in the QLD region,

Table 7: Models Performance on the **VIC** Dataset Across 24-Hour and 48-Hour Forecast Horizons.

Model	24H					48H				
	MAE	RMSE	sMAPE	rMAE	MDA	MAE	RMSE	sMAPE	rMAE	MDA
CNN-LSTM	75.013	467.766	83.663	0.74	61.965	86.816	476.73	92.741	0.856	54.954
DLinear	80.312	455.523	85.856	0.792	56.553	<u>82.740</u>	463.210	90.417	<u>0.816</u>	58.038
LSTM	75.213	471.492	83.876	0.742	<u>62.781</u>	84.0	476.018	90.79	0.829	<u>61.070</u>
Mamba	<u>73.153</u>	463.357	83.281	<u>0.722</u>	62.58	89.305	481.541	91.519	0.881	59.446
TimeMixer	80.238	459.176	80.919	0.791	60.843	89.804	477.208	<u>87.196</u>	0.886	59.833
TimeXer	71.859	<u>458.037</u>	77.753	0.709	60.375	78.752	468.272	84.690	0.777	59.161
TimesNet	77.484	462.307	<u>80.475</u>	0.764	63.338	85.632	<u>464.397</u>	89.019	0.845	59.926
Transformer	73.454	463.728	85.939	0.725	60.713	83.124	476.059	90.501	0.82	59.299
iTransformer	82.177	465.745	82.334	0.811	61.442	88.15	467.769	87.282	0.87	62.453

Note: Lower values indicate better performance, except for MDA, where higher values are preferred. MAE and RMSE are reported in Australian dollars (A\$/MWh). Best and second-best results are indicated in **bold** and underline, respectively.

where certain SOTA models, specifically TimeMixer (for both 24-hour and 48-hour horizons), TimesNet (48-hour), and DLinear (48-hour), record an rMAE above 1. This outcome indicates the weekly naïve model outperforms these specific models in the QLD market for those respective horizons. In contrast, linear models, such as DLinear and TimeMixer, generally underperform in most regions, highlighting their limited capability to model the nonlinear and highly volatile nature of electricity prices. Moreover, two other SOTA time series models, TimesNet and iTransformer, rarely appear among the top two performers.

Overall, across all regions and forecast horizons, the comparative evaluation shows that no single model universally dominates. The outcomes underscore that the optimal model choice is fundamentally linked to the unique volatility and overall stochastic characteristics of the specific regional market.

4.1.2. Overall Model Performance and Efficiency

Figure 3 presents the average performance of the evaluated models across all five NEM regions and both forecasting horizons. For the 24-hour horizon, CNN-LSTM, Mamba, and Transformer emerge as dominant performers. CNN-LSTM secured the top rank in sMAPE and MDA, while also placing second in MAE and third in RMSE. Mamba leads in MAE and rMAE, and is second-best in sMAPE. The Transformer ranks first in RMSE and third in MAE, rMAE, and MDA. Collectively, these three models occupy the ma-

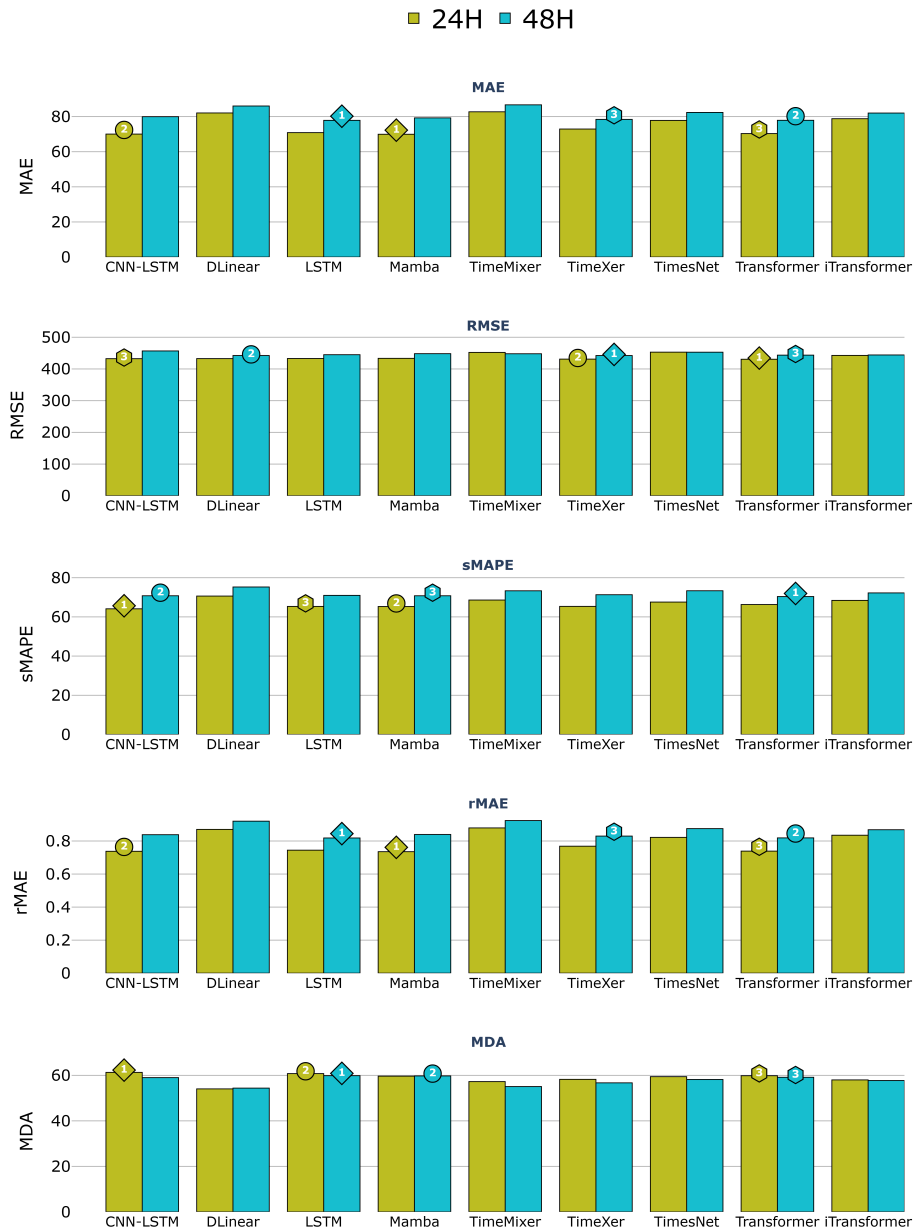


Figure 3: Average Performance of Models Across All Metrics.

jority of the top-three positions, outperforming SOTA time series models. Extending to the 48-hour horizon introduces greater diversity among top performers. TimeXer stands out prominently, achieving first place in RMSE and third place in MAE and rMAE. The Transformer maintains a competitive performance, ranking first in sMAPE and third in RMSE and MDA, while LSTM claims the top spot in MAE, rMAE, and MDA. In the longer horizon, two standard DL models, LSTM and Transformer, dominate overall, and only TimeXer shows promising results among the SOTA models. Overall, the standard DL models (LSTM, CNN-LSTM, Transformer) outperform the SOTA time series models in most cases across all metrics and horizons. Newer models, such as Mamba and TimeXer, have proven to be significant contenders, demonstrating superior performance in specific metrics.

Although accuracy remains the primary criterion for model evaluation, the training-time statistics in Figure 4 provide a complementary and important perspective. Lightweight architectures such as Mamba, LSTM, iTransformer, and DLinear exhibit substantially faster training times, often completing in a fraction of the time required by the more complex SOTA models. Among these, Mamba and LSTM stand out as particularly efficient, offering an excellent balance between performance and computational cost. The Transformer and CNN-LSTM require moderate training time yet de-

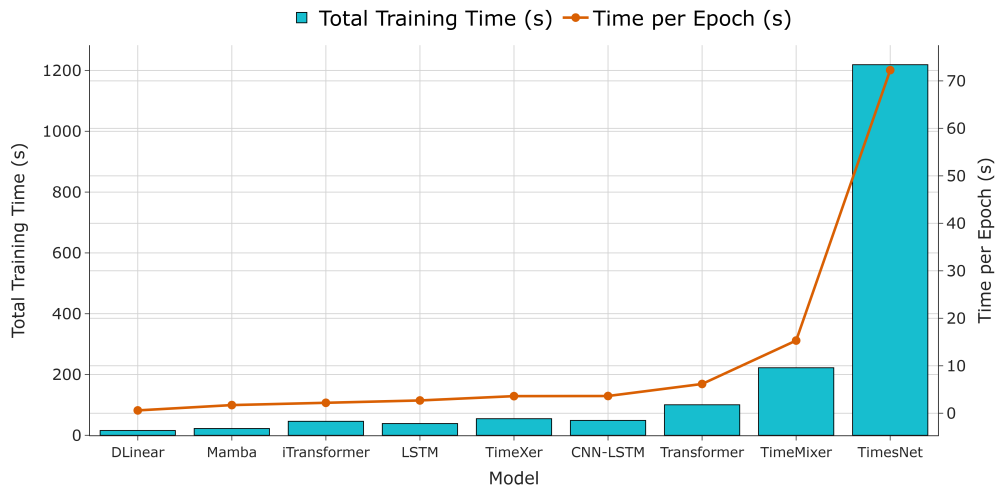


Figure 4: Training time (in seconds) of models for each forecast horizon.

liver consistently strong accuracy across both horizons. In contrast, the more computationally demanding models, TimeMixer and TimesNet, incur substantially higher total training times, yet these elevated costs are not matched by competitive forecasting performance. Both TimMixer and TimesNet fail to rank within the top three in any metric or horizon, resulting in a clearly unfavourable accuracy–efficiency trade-off. Overall, the balance between computational cost and forecasting performance of standard DL models in comparison to complex SOTA time series models suggests that architectural novelty alone does not guarantee superior performance.

4.1.3. Performance Degradation Analysis

Figure 5 shows the performance degradation percentage of each model. As expected, all models exhibit varying degrees of degradation, with a general trend of increasing MAE and sMAPE values. The CNN-LSTM shows the largest degradation, highlighting this hybrid network’s limited capacity to sustain accuracy under longer-range dependencies. Similarly, Mamba, Transformer, and LSTM experience substantial declines of approximately 10–13%. Despite ranking among the top performers, these models proved

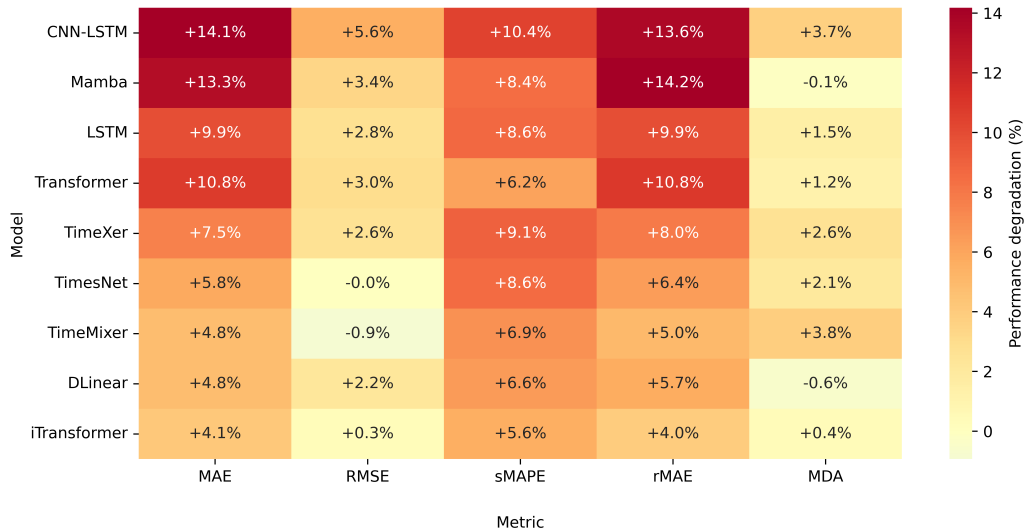


Figure 5: Performance degradation (%) for all models when extending the forecast horizon from 24H to 48H. Positive values denote performance degradation, whereas negative values indicate performance improvement.

Table 8: Statistical Summary of Regional Reference Price (RRP) at 5-min and 30-min Intervals

Dataset	5-min Interval						30-min Interval							
	μ	σ	Min	25%	50%	75%	Max	μ	σ	Min	25%	50%	75%	Max
QLD	101.947	420.073	-801.064	45.870	83.267	119.152	17500.000	101.947	336.859	-195.681	45.420	82.225	121.277	15631.376
NSW	115.674	545.631	-999.998	56.980	83.890	119.494	17500.000	115.674	459.463	-683.954	56.090	82.752	119.184	17500.000
VIC	74.544	332.302	-1000.000	8.230	61.793	115.913	17500.000	74.544	310.363	-686.552	5.595	62.298	115.886	16600.000
SA	92.758	484.672	-999.999	0.000	68.328	134.667	17500.000	92.758	413.774	-945.548	-1.831	68.985	133.472	16969.981
TAS	85.777	251.013	-998.068	30.280	70.200	120.100	17500.000	85.777	216.386	-922.399	31.148	71.394	120.080	16600.000

Note: μ : Mean; σ : Standard Deviation.

sensitive to horizon extension. Conversely, the SOTA time series models, particularly iTransformer, TimeMixer, and DLinear, although ranking lowest in error-based performance, exhibit remarkable robustness, with degradation rates below 5% in most cases. TimeXer occupies a balanced middle ground, performing competitively in error-based performance while also maintaining moderate degradation levels at longer horizons. Its deterioration is clearly less severe than that of CNN-LSTM, LSTM, Mamba, or the standard Transformer, though not as minimal as the most robust SOTA models. Interestingly, MDA values exhibited minimal degradation and even slight improvement for some models, indicating that while magnitude-based accuracy declines, trend prediction remains stable, a crucial property for trading strategies that rely on price movement direction rather than absolute value precision.

4.2. Regional Variation in Forecasting Error

The variation in forecasting performance across the regions of the NEM in Australia, as measured by MAE, RMSE, sMAPE, and MDA, reveals distinct patterns that appear consistent with differences in regional price characteristics (Table 8) and generation profiles. Figures 6-10 present 28-day generation statistics (%) for each NEM region, supporting the analysis and interpretation of performance variations and highlighting compositional differences across regions. These generation data cover the period from October 15, 2025, to November 12, 2025, and were collected from the Open Electricity⁸.

Absolute Error. For the 24-hour forecast horizon, TAS exhibits the lowest absolute errors (MAE, RMSE), followed by QLD. SA and NSW show the highest errors, with VIC falling in between. This ordering largely persists for the 48-hour horizon, although errors increase modestly across all regions.

⁸<https://openelectricity.org.au/>

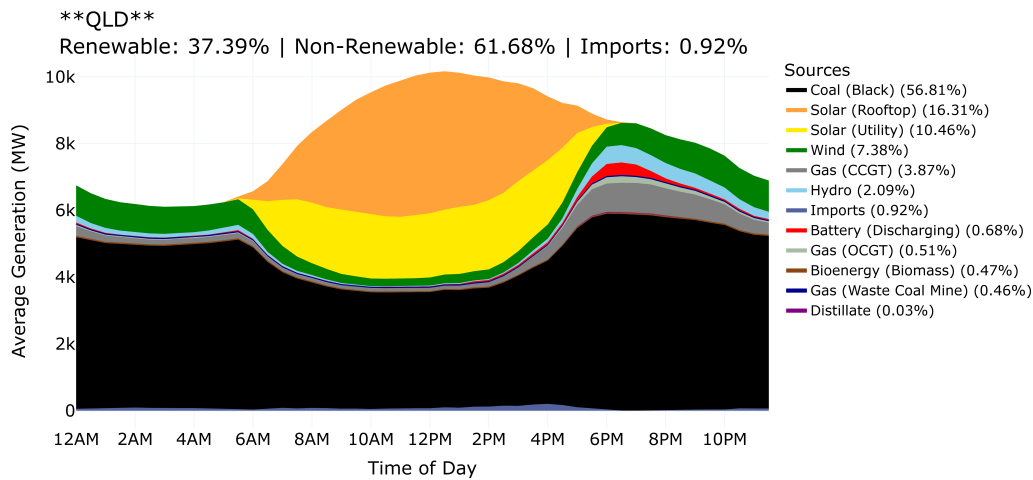


Figure 6: Diurnal generation profile for QLD by generation sources.

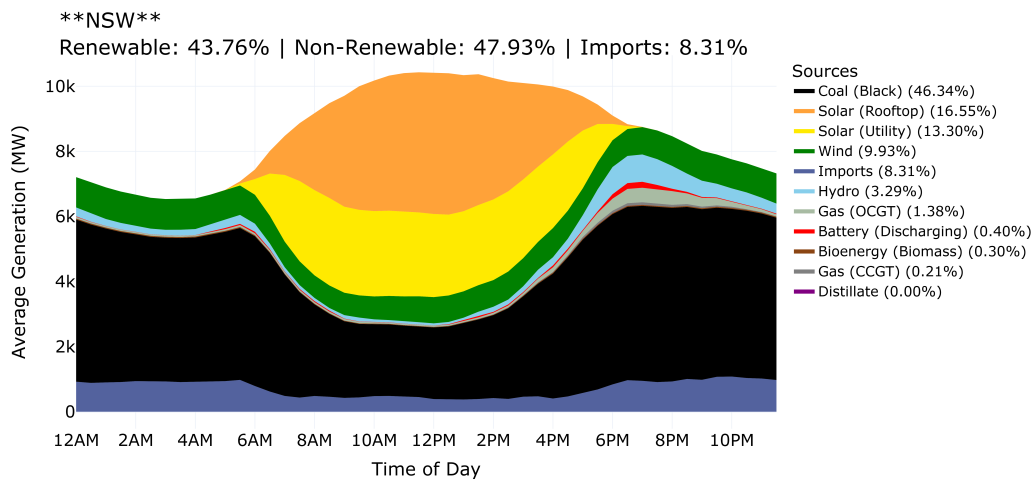


Figure 7: Diurnal generation profile for NSW by generation sources.

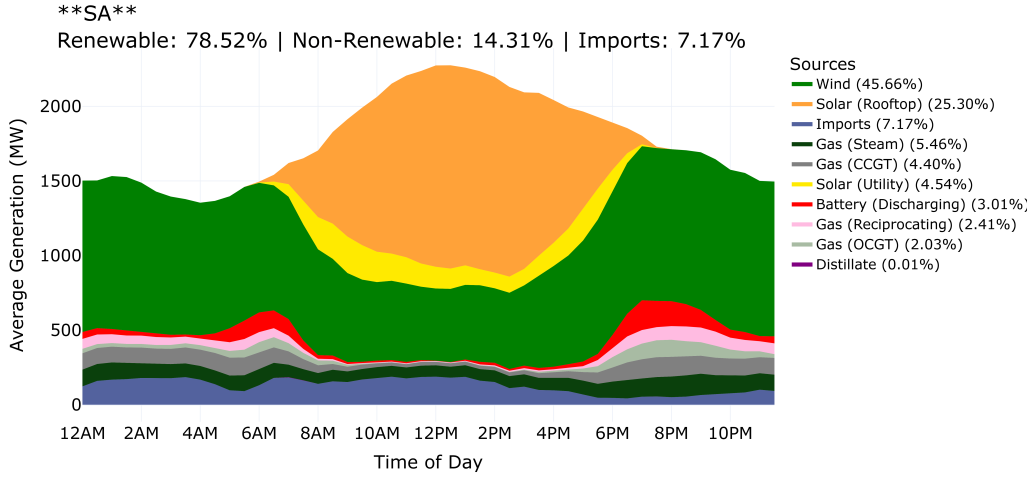


Figure 8: Diurnal generation profile for **SA** by generation sources.

The elevated MAE and RMSE in SA are primarily driven by higher price volatility stemming from its generation mix, which is dominated by intermittent renewable sources and reliance on imports. Notably, SA’s profile, which is heavily reliant on wind (45.66%) and solar (combined rooftop and utility: 29.84%), contributes to frequent periods of oversupply. This results in a substantial proportion of zero or near-zero prices, as indicated by its 25th percentile RRP at 5-minute intervals, during times of high renewable output. However, this intermittency also causes extreme price spikes during periods of low generation, reflected in SA’s wide RRP range and high standard deviation, which amplify absolute forecasting errors. Despite having a lower mean price than QLD and NSW (and only slightly higher than TAS), which might intuitively suggest lower errors, SA exhibits high MAE and RMSE. This indicates substantial forecasting difficulty, as models struggle to capture abrupt transitions from negative or zero prices to severe positive spikes driven by sudden supply shortages or demand surges. This highly asymmetric price distribution, characteristic of high renewable penetration, thus renders SA particularly challenging to forecast compared to regions with more balanced profiles.

A similar dynamic occurs in VIC, where the generation mix, featuring brown coal (46.63%) alongside substantial wind (22.99%) and solar (18.32%), fosters frequent low-price events. These conditions exacerbate forecasting er-

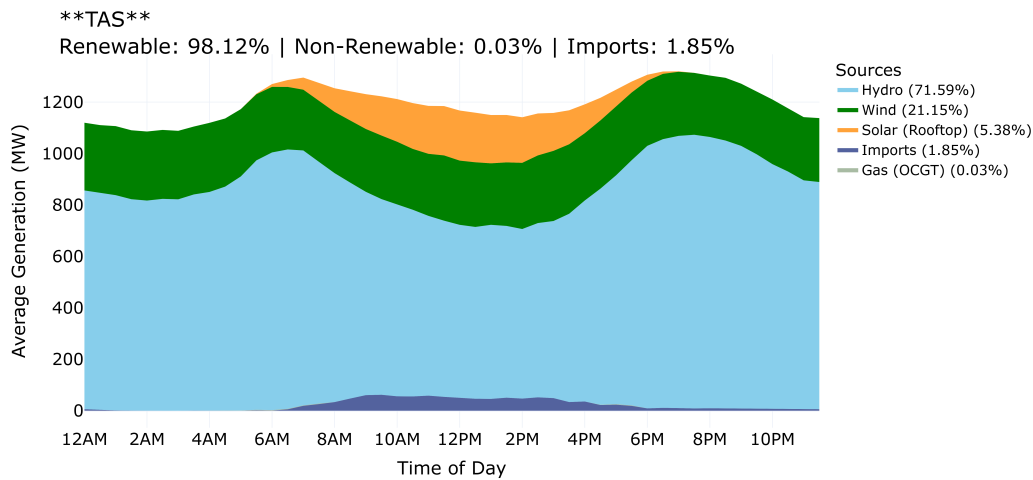


Figure 9: Diurnal generation profile for **TAS** by generation sources.

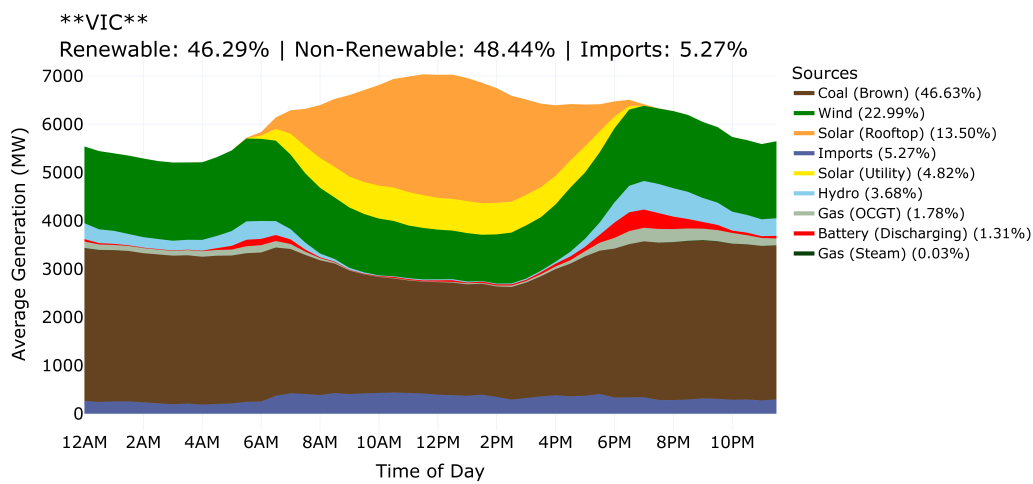


Figure 10: Diurnal generation profile for **VIC** by generation sources.

rors by producing unpredictable shifts between oversupply-induced negative or low prices and demand-driven highs. This explains why VIC’s MAE and RMSE exceed those of QLD, despite QLD having a higher mean price and standard deviation. VIC’s mean price is also lower than that of TAS, yet it records substantially larger absolute errors (more than 1.5 times higher). Although the percentile structure indicates that VIC prices do not display the same strong concentration in low and negative price intervals observed in SA, VIC’s 25th percentile remains comparatively low relative to all other regions except SA. This clustering does not mitigate the substantial forecast deviations observed. Instead, it obscures underlying distributional asymmetries, such as fat tails and abrupt intermittency-driven spikes, that generate larger errors than the region’s volatility level alone would imply.

In contrast, NSW exemplifies the expected relationship between price characteristics and forecasting error. The region shows the highest RMSE and second-highest MAE, aligning with its underlying price behavior: the highest mean prices and standard deviation among all regions, coupled with extreme upper-tail patterns. These traits are directly linked to NSW’s generation portfolio, which is dominated by black coal (46.34%) for baseload reliability but incorporates substantial variable renewables, solar (rooftop and utility combined: 29.85%), and wind (9.93%), alongside significant imports (8.31%). This mix enables extended periods of stable thermal output while still allowing sizable upward price excursions when renewable generation fluctuates or when imports introduce interconnected uncertainties. These dynamics drive both a higher mean price and elevated volatility, which in turn scale up absolute forecasting errors. Unlike regions with even higher renewable penetration but lower mean prices, and in some cases comparable or lower standard deviations, NSW exhibits forecasting challenges that are largely proportional to its price extremeness. In this context, forecasting difficulty arises not from frequent negative prices but from the amplified impact of extreme price spikes.

On the other hand, despite having a higher standard deviation than VIC, which is indicative of greater overall price variability, QLD’s MAE and RMSE are noticeably lower. QLD’s generation mix is heavily weighted toward black coal (56.81%), supplemented by rooftop solar (16.31%), utility solar (10.46%), and modest shares of wind and gas. The strong thermal baseload, alongside predictable diurnal solar patterns, yields price distributions that, although volatile, do not result in disproportionately large forecasting errors. The lower errors relative to volatility suggest that QLD’s price movements

are more predictable than those in VIC, SA, or NSW. Since MAE and RMSE directly quantify forecast deviations, their relatively smaller magnitudes indicate that the models capture QLD's price dynamics more effectively, despite the region's statistically wide price distribution.

TAS consistently demonstrates the lowest forecasting errors among all regions, as reflected by its MAE and RMSE values. These low errors are consistent with a stable generation profile dominated by hydro (71.59%), a dispatchable resource that provides consistent output and buffers against volatility. As a result, TAS displays the narrowest RRP distribution, evidenced by the lowest standard deviation, which in turn facilitates easier forecastability. Notably, although hydro is a renewable source, it is more predictable than solar or wind due to its dispatchable nature and storage capabilities.

Relative Error. Regarding sMAPE, which is particularly sensitive to errors at low or negative price levels due to its relative formulation, the metric shows pronounced elevation in SA and VIC compared to QLD and NSW, despite the latter's high absolute errors. This can be explained by the prevalence of low RRP values in SA and VIC, which increases the proportional impact of forecast inaccuracies near zero or negative prices, a common occurrence in high-renewable regions during periods of oversupply. Conversely, QLD and NSW, with higher 25th percentiles, experience less sMAPE inflation, as their price distributions are less affected by extreme low-price intervals despite overall volatility. TAS, with a relatively higher 25th percentile and hydro-driven stability, achieves the lowest sMAPE, further illustrating how generation profiles that minimise low-price occurrences facilitate superior relative forecasting performance.

Directional Accuracy. MDA, which evaluates the models' ability to correctly predict the direction of price changes, shows a markedly different pattern from MAE, RMSE, or sMAPE. When considering the best-performing models, TAS is the only region with MDA below 60%, reflecting the difficulty of predicting directional changes in a hydro-dominated market where price movements are small in magnitude and therefore resemble noise. In contrast, QLD, VIC, SA, and NSW all achieve MDA values above 60%, and the differences between these regions are relatively small, particularly when compared to the large disparities in absolute and relative errors. This suggests that, while TAS presents a unique challenge for directional forecasting,

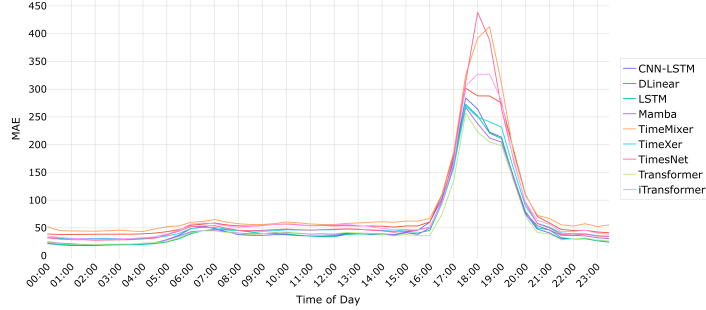
the remaining regions demonstrate a different pattern. Although absolute errors vary substantially due to regional differences in price distributions and volatility, the models are nonetheless able to capture the overall direction of price movements with comparable, though not identical, effectiveness across regions. Consequently, MDA is less sensitive to regional differences in volatility and price extremes, indicating that directional predictability remains relatively consistent across most NEM regions, even when forecasting absolute price magnitudes proves challenging.

4.3. Diurnal Performance Patterns

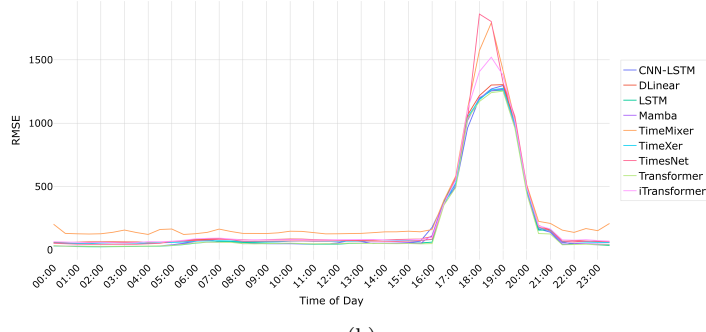
To gain deeper insights into the temporal dynamics of the price forecasting accuracy, we conducted a granular analysis of model performance across the 48 half-hour intervals of the day. By evaluating all the models at each time interval, we uncover how diurnal cycles in electricity generation, renewable output variability, and price behaviour influence forecasting challenges. This time-centric perspective complements the model- and region-focused discussions above, revealing that price forecasting difficulty is not uniform throughout the day but clusters around specific periods driven by underlying market mechanics. All NEM regions show broadly comparable diurnal patterns in forecasting performance. Therefore, for illustrative clarity and analytical conciseness, we restrict our detailed discussion to the QLD region as a representative case. Comprehensive diurnal performance visualisations for the remaining NEM regions are provided in the Appendix B.

4.3.1. Absolute Errors Spike Driven by High Evening Volatility

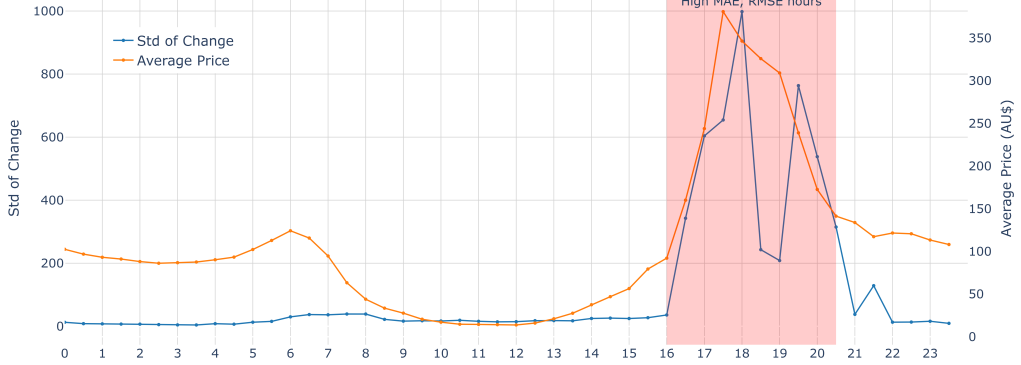
The absolute error metrics, MAE and RMSE (Figures 11(a) and 11(b)), demonstrate pronounced diurnal patterns, with performance degradation concentrated in specific high-volatility windows. As illustrated in Figure 11(c), which plots the standard deviation of price changes (blue line) alongside the average price (orange line) for each half-hour interval, error peaks in MAE and RMSE align closely with periods of elevated short-term price volatility. These high-volatility hours, spanning approximately 16:00 to 20:30, correspond to the evening ramp-up in demand as solar generation wanes, a hallmark of QLD’s solar-heavy profile. Although MAE and RMSE increase for all models during the evening volatility window, the rise is comparatively modest for sequence-based architectures such as Transformers, Mamba, and LSTM, whereas models like TimeMixer, TimesNet, and others experience noticeably larger error escalations. During this transition, the standard deviation of



(a)



(b)



(c)

Figure 11: Interval-level absolute forecasting errors and diurnal price characteristics for the **QLD** region. (a) MAE of all models for a 24H forecast horizon, evaluated at 30-minute intervals. (b) RMSE of all models for a 24H forecast horizon, evaluated at 30-minute intervals. (c) Diurnal electricity price dynamics, showing standard deviation of price changes and average price, with the shaded region (16:00–20:30) indicating periods of elevated forecasting errors.

price changes surges dramatically, reaching up to 1000 A\$/MWh. This surge reflects abrupt shifts as dispatchable sources, including coal, gas, and battery discharges, ramp up to offset declining solar output. Batteries, in particular, can either discharge or charge, contributing to rapid, nonlinear price fluctuations. This behaviour intensifies short-term volatility, making these hours inherently challenging and amplifying forecasting errors as models struggle to capture the resulting dynamics. The average price curve further contextualises this, showing a dip during solar peaks (around 7:00–15:00), reflecting the low marginal cost associated with abundant solar generation, followed by a rapid increase during the evening ramp-up.

Conversely, stable periods such as early morning (00:00–06:00) and late night (21:00–23:30) exhibit minimal volatility, with standard deviations consistently below 100 A\$/MWh. This stability results in significantly lower MAE and RMSE during those periods. This contrast is fundamentally driven by the market’s generation profile. During these stable hours, variable renewable generation is minimal compared to the daytime, and the electricity supply is dominated by consistent, baseload coal generation. This stable composition reduces the need for rapid system balancing, which otherwise drives price volatility.

Extending this to a 48-hour forecasting horizon would likely compound these effects, as cumulative uncertainties from renewable intermittency propagate, aligning with the modest increases in MAE and RMSE in Section 4.2.

4.3.2. *Relative Errors Inflate Driven by Midday Negative Price Regimes*

Relative error, as measured by sMAPE (Figure 12(a)), reveals a distinct but complementary diurnal profile, with degradation tied not just to volatility but to the prevalence of low or negative prices. Figure 12(b) overlays the average price (orange line) with the percentage of negative prices (pink bars) across intervals, highlighting “high sMAPE hours” in light blue where errors are most pronounced. sMAPE spikes dramatically during midday intervals (roughly 07:00–16:00), coinciding with peak negative price occurrences exceeding 40% in some slots, a consequence of QLD’s solar oversupply. When solar generation floods the market, as evident in the generation stack area plot (Figure 6), where the orange and yellow solar layers dominate during midday, prices often fall below zero to incentivise consumption or curtailment. sMAPE’s formula, which normalises errors by the average of actual and predicted values, becomes highly sensitive when prices hover near zero, such that even modest absolute deviations translate into large relative errors.

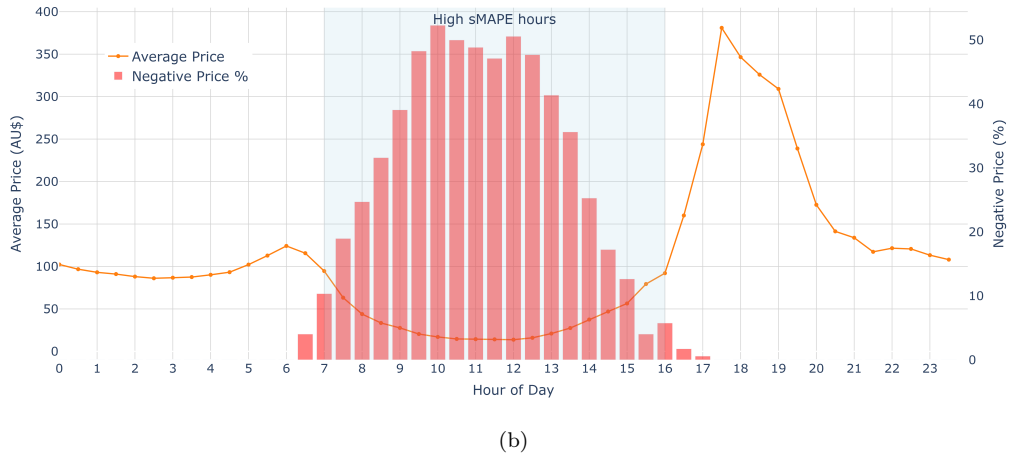
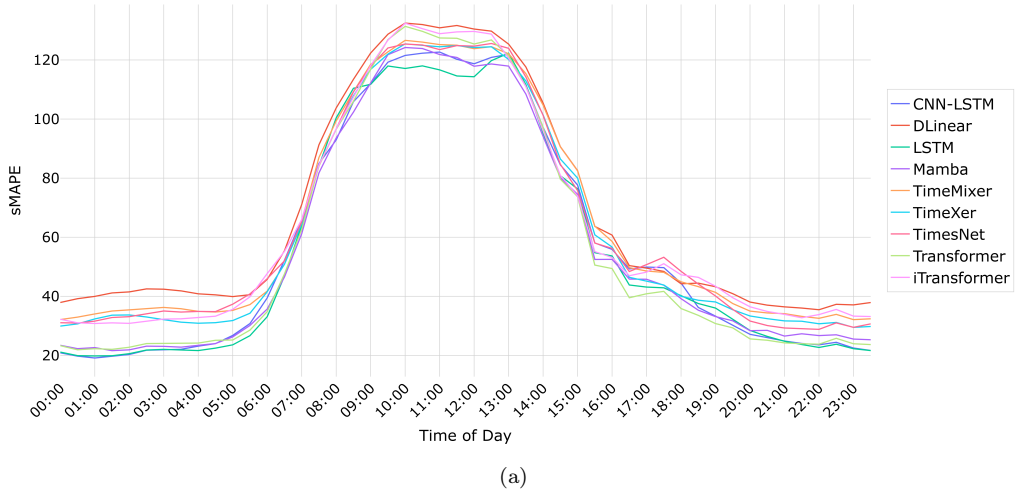


Figure 12: (a) sMAPE of all models on the **QLD** region for a 24H forecast horizon, evaluated at 30-minute intervals. (b) Diurnal electricity price patterns in the **QLD** region. The line represents the average price per 30-minute interval across all days, while the bars indicate the percentage of negative prices at each interval. The shaded region (07:00–16:00) highlights the hours with higher sMAPE.

Outside these hours, sMAPE stabilises, particularly during evening peaks when average prices rise above 200 A\$/MWh and negative incidences drop to near zero. This stability benefits from QLD's substantial coal baseload, which contributes to more stable supply conditions and dampens extreme downward price movements during high-demand periods. The key outcome here is that sMAPE degradation is disproportionately driven by negative pricing intervals, which are amplified by high VRE penetration (e.g., solar at 26.77% and wind at 7.38%), rather than pure volatility. This helps explain why regions like SA, with even higher VRE shares (over 75%), face elevated sMAPE overall (Section 4.2). Accordingly, these outcomes suggest that models with explicit mechanisms for handling negative prices are necessary to mitigate these higher errors in wind- and solar-rich markets.

4.3.3. Directional Accuracy Degradation during Periods of Frequent Price Shifts

Directional accuracy, quantified by MDA (Figure 13(a)), displays pronounced diurnal oscillations, with multiple dips corresponding to periods of frequent price direction changes. Figure 13(b) illustrates the percentage of directional shifts in the actual data (red line). Low MDA hours (highlighted in pink) correspond to intervals of high directional instability, where the sign of price changes frequently flips, often exceeding 40%, reflecting erratic trends that challenge forecasting models. These patterns are closely linked to QLD's generation dynamics, as shown in the generation stack area plot (Figure 6).

The diurnal variations can be broadly classified into unstable and stable periods. Unstable periods, with frequent directional shifts and low MDA, occur during early morning (01:30–04:30), late morning to early afternoon (08:30–15:00), and late evening (22:00–23:00), consistent with transitions in renewable output and minor adjustments in gas, hydro, or battery dispatch. Stable periods, in contrast, show smoother price trends and higher MDA. These include mid-morning (05:00–08:00), when directional shifts are lower and coincide with the gradual solar increase before peak intensity; and evening (15:30–21:30), where a strong upward price trend—accompanied by steadier baseload and dispatchable output—aligns with directional shifts frequently below 40%, during which MDA often exceeds 70%. These patterns indicate that forecasting models achieve higher directional accuracy when supply and demand are more consistent, while periods of transitional generation present greater challenges.

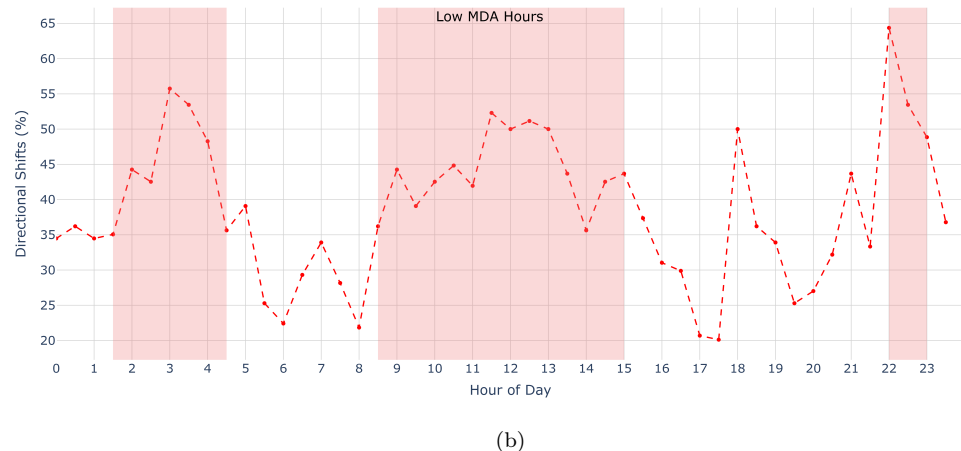
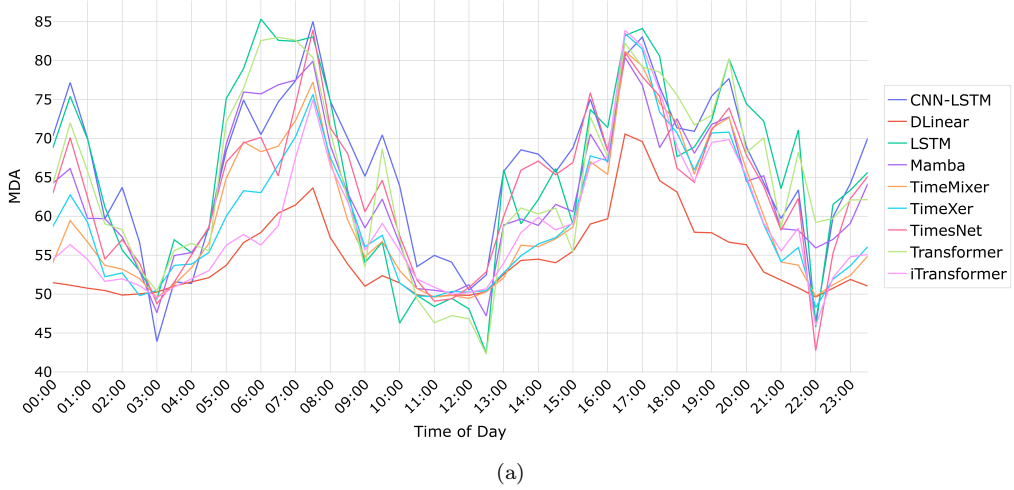


Figure 13: (a) MDA of all models on the **QLD** region for a 24H forecast horizon, evaluated at 30-minute intervals. (b) The percentage of directional shifts for each interval in the **QLD** region is represented by a red dashed line. Shaded regions indicate the hours with the low MDA, highlighting periods of reduced directional forecasting performance associated with rapid directional changes.

4.4. Discussion

A notable outcome of this study is that standard DL baselines, specifically LSTM, CNN-LSTM, and the standard Transformer, demonstrate superior performance relative to the six recent SOTA time series architectures evaluated across multiple NEM regions and forecast horizons. This challenges the prevailing expectation that specialised long-sequence forecasting models should inherently deliver superior performance due to their advanced temporal modelling mechanisms.

The following subsections examine the implications from the perspectives of feature representation, model design, and optimisation objectives.

4.4.1. Additional Feature Integration and Effective Representation

This study approached EPF as a univariate time series task, relying solely on historical prices. This design allowed a controlled comparison of model behaviour across regions and horizons. However, the results reveal a significant discrepancy between trend prediction and magnitude estimation. As noted in Section 4.2, while directional accuracy remained relatively stable across all regions (above 60% for most), the magnitude-based error varied substantially. This suggests that while historical price data capture the general inertia of market movement, they do not encapsulate the underlying drivers of extreme deviations.

The primary limitation is the absence of explanatory features reflecting the physical generation mix described in Section 4.2. For instance, the diurnal analysis (Section 4.3.2) showed that in QLD, sMAPE spikes occur during midday due to solar oversupply and negative pricing, while RMSE spikes occur during the evening ramp as dispatchable generation replaces solar output. A univariate model observes these solely as statistical variations. Without explicit inputs, such as solar irradiance forecasts to capture the midday dip or thermal availability to anticipate the evening spike, the model responds reactively rather than anticipatively. Similarly, elevated sMAPE values in SA and VIC arise from zero-price events caused by renewable saturation; without generation information, the model cannot distinguish these events from periods of low demand.

Future work should therefore transition from univariate inputs to multivariate representations. The challenge extends beyond simply adding more variables; it requires representations that properly account for the distinct temporal alignment of these features. As shown in the results, price volatility exhibits a bimodal structure (midday solar lows vs evening demand highs).

Future models should integrate additional data, such as weather, interconnector flows, generation, and load, in ways that enable anticipation of these structural shifts, rather than relying on past price momentum, which breaks down during the rapid transitions observed during the evening ramp.

4.4.2. Balancing Short-Term Sensitivity and Long-Term Robustness in Model Design

While Section 4.1 demonstrates that standard DL models generally outperform SOTA time series models in short-term accuracy, the degradation analysis in Section 4.1.3 reveals a critical trade-off between local sensitivity and global robustness. A distinctive dichotomy emerged in the results: models that achieved the lowest errors in the 24-hour horizon, such as CNN-LSTM and LSTM, exhibited the highest rates of performance degradation as the horizon extended to 48 hours.

This divergence highlights the cost associated with the local sensitivity discussed earlier. Standard DL models, particularly the hybrid CNN-LSTM, rely heavily on high-frequency variations and immediate price momentum. While this inductive bias makes them exceptionally effective at modelling the jagged dynamics of the NEM, it leads to rapid error accumulation over longer horizons. As observed in the results, these models experience degradation rates of approximately 10–13% as the forecast window extends. This suggests that the local volatility signals they prioritise are transient; as the immediate context decays over 48 hours, the models lack the long-range structural representations required to maintain stability.

In contrast, most SOTA time series DL architectures, such as iTransformer and TimeMixer, demonstrated superior stability—with degradation rates often below 5%—but failed to rank competitively in absolute error metrics. This indicates that their stability likely stems from an “over-smoothing” of the data, effectively filtering out the high-frequency volatility that characterises the 24-hour NEM market in favour of capturing longer-term, albeit less precise, trends. TimeXer emerged as a notable exception, effectively bridging this gap by maintaining competitive error-based performance while exhibiting only moderate degradation. This suggests that its architecture, which mixes temporal patches, manages to capture a more durable representation of the price signal than the purely recurrent baselines without succumbing to the excessive smoothing seen in other SOTA models.

Consequently, future work should prioritise the development of architectures that are simultaneously effective at capturing short-term volatility

and robust over long forecasting horizons. A promising direction lies in decomposing the forecasting task: utilising convolutional or recurrent modules to capture short-term, high-frequency residuals (volatility), while leveraging attention-based or decomposition-based SOTA components to model the stable, long-range trend. Such a coupled approach would aim to retain the superior short-term accuracy while inheriting the horizon-robustness of modern time series architectures.

4.4.3. Optimisation Objectives for Asymmetric and Heavy-Tailed Price Distributions

All models in this study were optimised using the MSE loss function, the standard choice for point forecasting. While MSE performs well for general regression tasks, the results in Sections 4.3.1 and 4.3.2 highlight its limitations when applied to the distributional characteristics of NEM prices. sMAPE degradation during midday periods in solar-rich regions reflects the prevalence of zero and negative prices, where even small absolute deviations translate into disproportionately large relative errors. Because MSE is symmetric in the error term and invariant to price magnitude, it assigns equal penalty across regimes and therefore under-emphasises those intervals where forecasting is most challenging.

In markets with highly skewed and heavy-tailed price distributions, such as NEM, frequent negative prices coupled with occasional extreme spikes encourage models to regress toward the mean. This results in smoothing over sharp dips and under-learning the dynamics that govern both negative-price intervals and extreme spikes. While such behaviour is mathematically consistent with symmetric error minimisation, it is misaligned with the operational importance of accurately forecasting outcomes at both tails of the price distribution.

Future work may therefore explore loss functions tailored to the asymmetric and heavy-tailed nature of electricity prices, including asymmetric or regime-weighted objectives, or stabilised relative-error formulations. Such approaches would better align the optimisation objective with the economic and operational significance of forecasting both negative-price events and scarcity-driven spikes.

5. Conclusion

This study proposes a novel EPF framework for day-ahead and two-day-ahead forecasting across all five regions of the NEM. Within this framework, we adopt standard DL architectures—namely, LSTM, CNN–LSTM, and Transformer models—together with six recent SOTA time series forecasting DL models. The results indicate that no single model consistently outperforms others across all regions and forecasting horizons. However, standard DL baselines overall deliver better performance across most regions and horizons. In contrast, several new architectures, despite their sophistication, show less effectiveness at capturing the heavy-tailed volatility and rapid transitions characteristic of renewable-driven markets. Nevertheless, SOTA time series models exhibit greater robustness to horizon extension, with minimal performance degradation compared to the baseline DL models.

The results also highlighted substantial regional variation in forecasting error, shaped by generation portfolios and distributional characteristics of price rather than volatility magnitude alone. The analysis reveals that regions with high VRE penetration, such as SA and VIC, pose greater challenges due to the frequent occurrence of negative prices and extreme spikes. At the same time, hydro-dominated TAS yields the lowest errors. The diurnal performance patterns driven by evening ramp volatility, midday negative pricing, and directional instability further highlight the influence of market mechanics, revealing specific time-of-day windows in which forecast reliability is most at risk.

The implications of these findings extend beyond the comparative analysis of model performance. First, the study highlights the limitations of univariate price forecasting. It underscores the need for multivariate representations that better capture the physical and operational drivers of price formation. Second, the absence of a universally dominant architecture across volatility regimes suggests that future work should move beyond selecting a single winner and instead focus on integrating complementary modelling capabilities. The results motivate the exploration of hybrid frameworks that balance sensitivity to high-frequency volatility with robustness under longer-term forecasting, rather than relying on a single architectural paradigm. Finally, the challenges encountered under negative-price regimes and extreme scarcity events necessitate loss formulations that more accurately capture the asymmetric and heavy-tailed nature of electricity prices. Future research would therefore benefit from integrating richer feature representations, developing

modelling strategies that enhance robustness under longer-term forecasting, and exploring optimisation objectives beyond symmetric global error minimisation. Together, these findings provide a rigorous foundation for advancing EPF methodologies and guiding the design of forecasting models that more effectively accommodate regional diversity, operational realities, and the volatility regimes of renewable-integrated power systems.

CRediT authorship contribution statement

Mohammed Osman Gani: Conceptualisation, Methodology, Software, Investigation, Writing—original draft, Writing—review & editing, Visualisation. **Zhipeng He:** Methodology, Software, Investigation, Writing—review & editing. **Chun Ouyang:** Methodology, Investigation, Supervision, Writing—review & editing. **Sara Khalifa:** Methodology, Supervision, Writing—review & editing.

Declaration of competing interest

The authors declare that they have no known competing financial interests or personal relationships that could have appeared to influence the work reported in this paper.

Data availability

Data will be made available on request.

Acknowledgements

The reported research forms part of a PhD project supported by the QUT Postgraduate Research Award (QUTPRA) at Queensland University of Technology (QUT), Australia.

Funding sources

This research did not receive any specific grant from funding agencies in the public, commercial, or not-for-profit sectors.

Declaration of generative AI and AI-assisted technologies in the manuscript preparation process

During the preparation of this work, the authors used ChatGPT to improve the clarity, grammar, and coherence of the writing. After using this tool, the authors reviewed and edited the content as necessary and take full responsibility for the content of the published article.

Appendix A. Hyperparameter Search Results

Table A.1: Optimal Hyperparameters for Dataset **QLD** (Dim: Hidden Dimensions; F. Size: Filter Size; Filters: Number of Filters, LR: Learning Rate; N. Layers: Number of Layers.)

Forecast Horizon	Model	Dim.	F. Size	Filters	LR	N. Layers
48	CNN-LSTM	128	7	64	0.001	-
	DLinear	-	-	-	0.001	-
	LSTM	256	-	-	0.001	1
	Mamba	64	-	-	0.005	-
	TimeMixer	32	-	-	0.001	2
	TimeXer	32	-	-	0.005	2
	TimesNet	256	-	-	0.001	2
	Transformer	32	-	-	0.001	2
	iTransformer	32	-	-	0.005	2
	CNN-LSTM	128	7	32	0.005	-
96	DLinear	-	-	-	0.001	-
	LSTM	64	-	-	0.005	2
	Mamba	32	-	-	0.01	-
	TimeMixer	256	-	-	0.001	2
	TimeXer	64	-	-	0.001	2
	TimesNet	32	-	-	0.005	2
	Transformer	256	-	-	0.001	2
	iTransformer	32	-	-	0.001	1

Table A.2: Optimal Hyperparameters for Dataset **NSW** (Dim: Hidden Dimensions; F. Size: Filter Size; Filters: Number of Filters, LR: Learning Rate; N. Layers: Number of Layers.)

Forecast Horizon	Model	Dim.	F. Size	Filters	LR	N. Layers
48	CNN-LSTM	128	3	128	0.01	-
	DLinear	-	-	-	0.001	-
	LSTM	32	-	-	0.1	1
	Mamba	32	-	-	0.005	-
	TimeMixer	32	-	-	0.001	2
	TimeXer	64	-	-	0.001	2
	TimesNet	64	-	-	0.001	2
	Transformer	64	-	-	0.001	2
	iTransformer	32	-	-	0.001	1
96	CNN-LSTM	512	3	64	0.001	-
	DLinear	-	-	-	0.001	-
	LSTM	32	-	-	0.001	2
	Mamba	64	-	-	0.001	-
	TimeMixer	128	-	-	0.001	2
	TimeXer	128	-	-	0.001	2
	TimesNet	128	-	-	0.001	1
	Transformer	32	-	-	0.001	2
	iTransformer	32	-	-	0.001	2

Table A.3: Optimal Hyperparameters for Dataset **SA** (Dim: Hidden Dimensions; F. Size: Filter Size; Filters: Number of Filters, LR: Learning Rate; N. Layers: Number of Layers.)

Forecast Horizon	Model	Dim.	F. Size	Filters	LR	N. Layers
48	CNN-LSTM	128	5	32	0.001	-
	DLinear	-	-	-	0.001	-
	LSTM	256	-	-	0.005	2
	Mamba	32	-	-	0.01	-
	TimeMixer	32	-	-	0.001	2
	TimeXer	32	-	-	0.001	2
	TimesNet	32	-	-	0.005	1
	Transformer	128	-	-	0.001	2
96	iTransformer	64	-	-	0.001	1
	CNN-LSTM	512	3	512	0.01	-
	DLinear	-	-	-	0.001	-
	LSTM	64	-	-	0.1	1
	Mamba	32	-	-	0.001	-
	TimeMixer	512	-	-	0.001	2
	TimeXer	32	-	-	0.005	2
	TimesNet	512	-	-	0.001	1
	Transformer	64	-	-	0.005	1
	iTransformer	256	-	-	0.001	2

Table A.4: Optimal Hyperparameters for Dataset **TAS** (Dim: Hidden Dimensions; F. Size: Filter Size; Filters: Number of Filters, LR: Learning Rate; N. Layers: Number of Layers.)

Forecast Horizon	Model	Dim.	F. Size	Filters	LR	N. Layers
48	CNN-LSTM	128	3	128	0.005	-
	DLinear	-	-	-	0.001	-
	LSTM	128	-	-	0.001	1
	Mamba	32	-	-	0.001	-
	TimeMixer	32	-	-	0.001	2
	TimeXer	64	-	-	0.001	1
	TimesNet	32	-	-	0.001	2
	Transformer	32	-	-	0.005	2
	iTransformer	64	-	-	0.001	2
96	CNN-LSTM	128	3	64	0.005	-
	DLinear	-	-	-	0.001	-
	LSTM	128	-	-	0.01	1
	Mamba	32	-	-	0.001	-
	TimeMixer	32	-	-	0.001	2
	TimeXer	32	-	-	0.001	1
	TimesNet	512	-	-	0.001	1
	Transformer	32	-	-	0.01	2
	iTransformer	64	-	-	0.01	2

Table A.5: Optimal Hyperparameters for Dataset **VIC** (Dim: Hidden Dimensions; F. Size: Filter Size; Filters: Number of Filters, LR: Learning Rate; N. Layers: Number of Layers.)

Forecast Horizon	Model	Dim.	F. Size	Filters	LR	N. Layers
48	CNN-LSTM	64	3	128	0.005	-
	DLinear	-	-	-	0.001	-
	LSTM	32	-	-	0.005	2
	Mamba	32	-	-	0.005	-
	TimeMixer	64	-	-	0.001	2
	TimeXer	64	-	-	0.001	1
	TimesNet	32	-	-	0.001	2
	Transformer	512	-	-	0.001	2
	iTransformer	128	-	-	0.001	1
96	CNN-LSTM	32	7	128	0.05	-
	DLinear	-	-	-	0.001	-
	LSTM	128	-	-	0.01	2
	Mamba	128	-	-	0.001	-
	TimeMixer	64	-	-	0.001	2
	TimeXer	32	-	-	0.005	2
	TimesNet	128	-	-	0.001	1
	Transformer	256	-	-	0.001	2
	iTransformer	32	-	-	0.001	2

Appendix B. Diurnal Performance

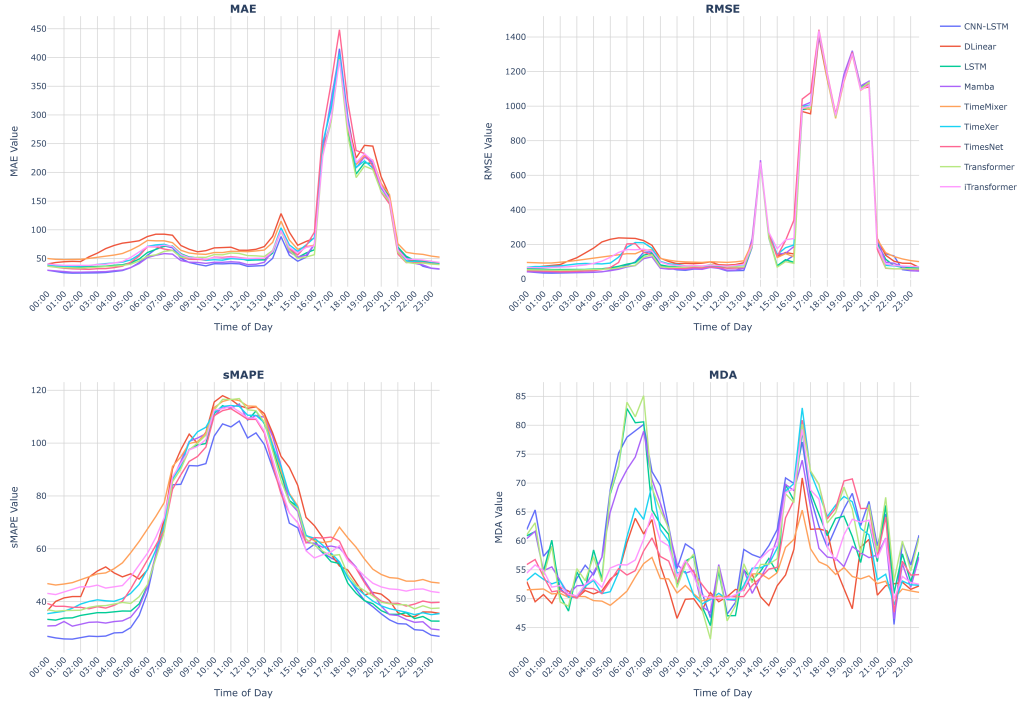


Figure B.1: MAE, RMSE, sMAPE, and MDA of each interval of the day in the **NSW** region for all the evaluated models.

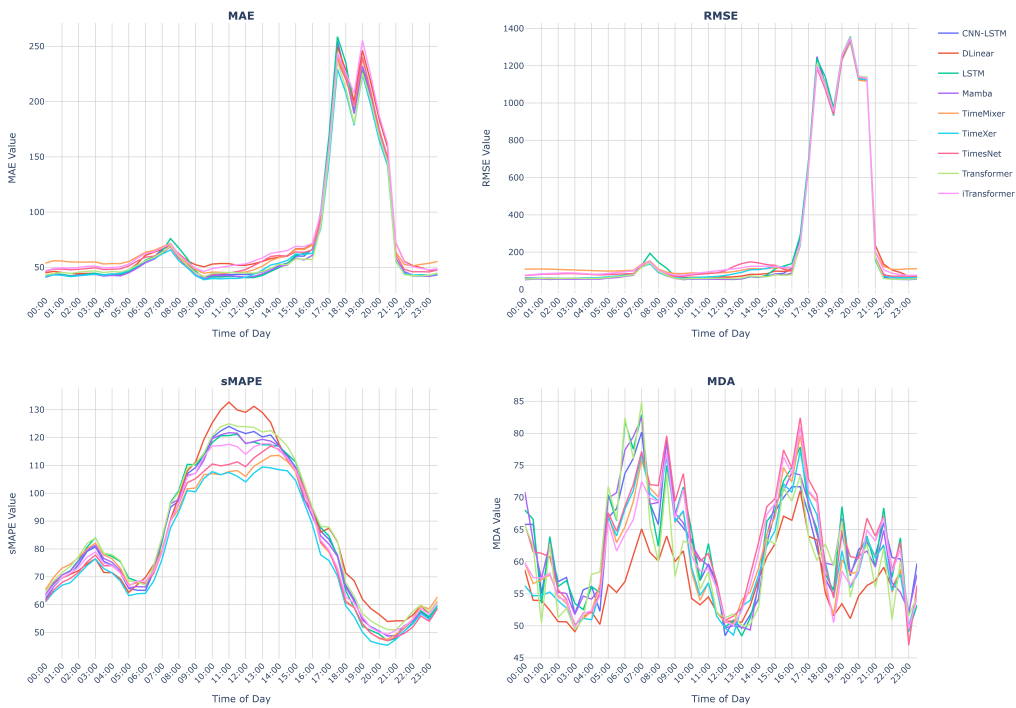


Figure B.2: MAE, RMSE, sMAPE, and MDA of each interval of the day in the **VIC** region for all the evaluated models.

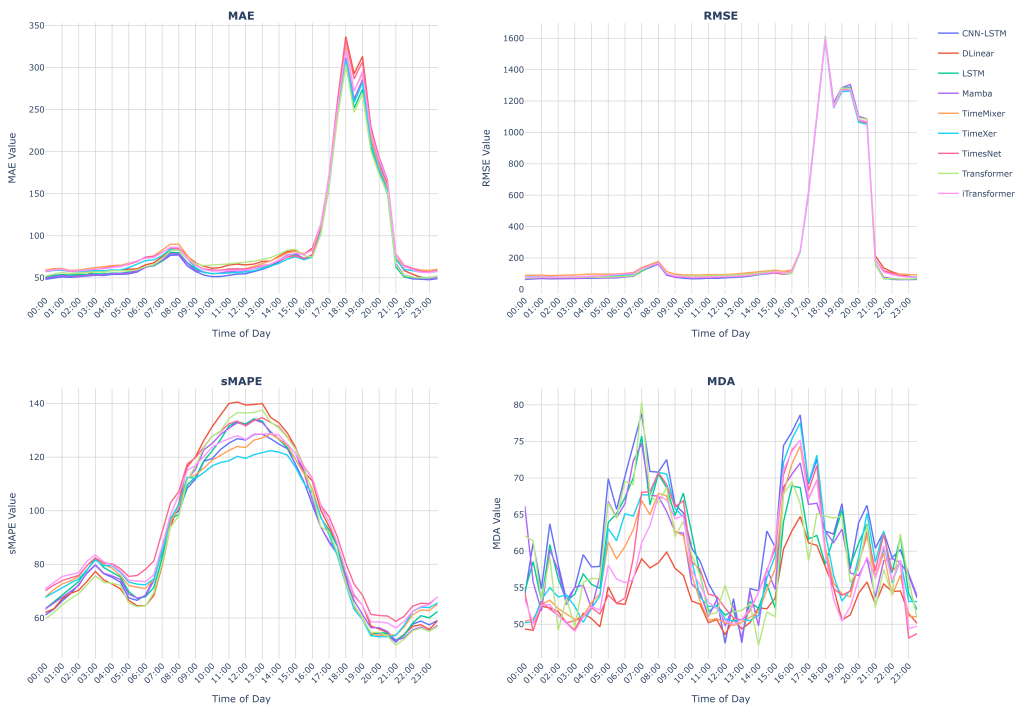


Figure B.3: MAE, RMSE, sMAPE, and MDA of each interval of the day in the **SA** region for all the evaluated models.

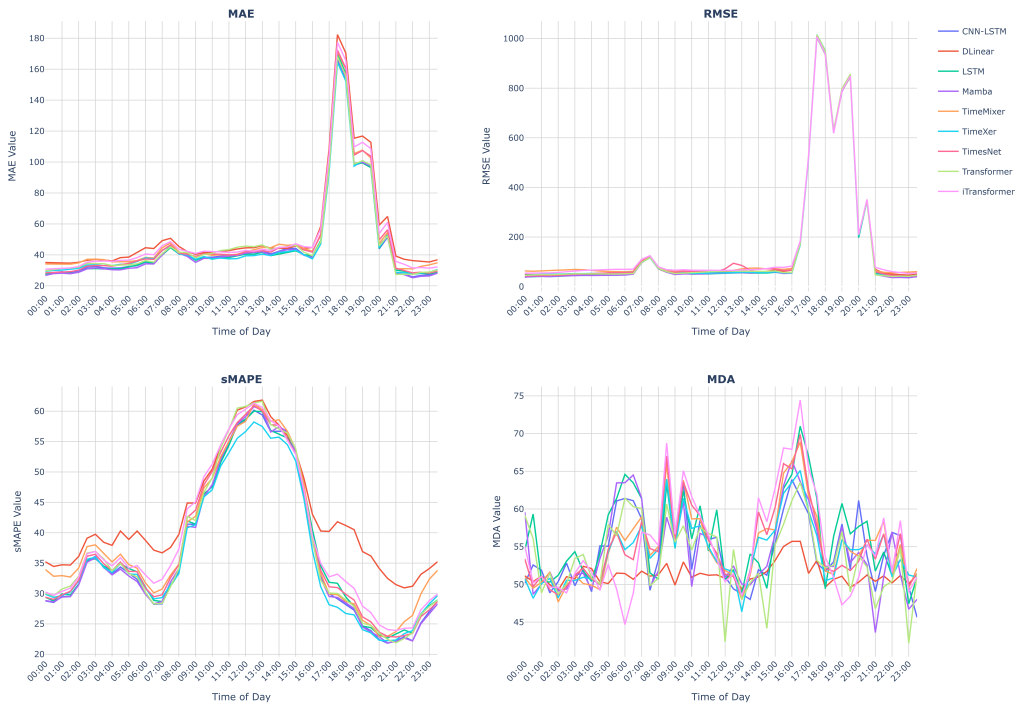


Figure B.4: MAE, RMSE, sMAPE, and MDA of each interval of the day in the **TAS** region for all the evaluated models.

References

- [1] C. O'Connor, M. Bahloul, R. Rossi, S. Prestwich, A. Visentin, Conformal prediction for electricity price forecasting in the day-ahead and real-time balancing market, *Energy and AI* 21 (2025) 100571. <https://doi.org/10.1016/j.egyai.2025.100571>.
- [2] S. Ghimire, R. C. Deo, K. Hopf, H. Liu, D. Casillas-Pérez, A. Hellwig, S. S. Prasad, J. Pérez-Aracil, P. D. Barua, S. Salcedo-Sanz, Half-hourly electricity price prediction model with explainable-decomposition hybrid deep learning approach, *Energy and AI* 20 (2025) 100492. <https://doi.org/10.1016/j.egyai.2025.100492>.
- [3] V. Laitkos, G. Vontzos, P. Paraschoudis, E. Tsampasis, D. Bargiolas, L. H. Tsoukalas, The state of the art electricity load and price forecasting for the modern wholesale electricity market, *Energies* 17 (2024) 5797. <https://doi.org/10.3390/en17225797>.
- [4] J. Nyangon, R. Akintunde, Principal component analysis of day-ahead electricity price forecasting in CAISO and its implications for highly integrated renewable energy markets, *Wiley Interdiscip. Rev. Energy Environ.* 13 (2024) e504. <https://doi.org/10.1002/wene.504>.
- [5] J. Lago, F. De Ridder, B. De Schutter, Forecasting spot electricity prices: Deep learning approaches and empirical comparison of traditional algorithms, *Appl. Energy* 221 (2018) 386–405. <https://doi.org/10.1016/j.apenergy.2018.02.069>.
- [6] R. Weron, Electricity price forecasting: A review of the state-of-the-art with a look into the future, *Int. J. Forecast.* 30 (2014) 1030–1081. <https://doi.org/10.1016/j.ijforecast.2014.08.008>.
- [7] M. Gürtler, T. Paulsen, Forecasting performance of time series models on electricity spot markets: a quasi-meta-analysis, *Int. J. Energy Sect. Manage.* 12 (2018) 103–129. <https://doi.org/10.1108/IJESM-06-2017-0004>.
- [8] A. J. Conejo, M. A. Plazas, R. Espinola, A. B. Molina, Day-ahead electricity price forecasting using the wavelet transform and ARIMA models, *IEEE Trans. Power Syst.* 20 (2005) 1035–1042. <https://doi.org/10.1109/tpwrs.2005.846054>.

- [9] D. H. Mazengia, L. A. Tuan, Forecasting spot electricity market prices using time series models, in: 2008 IEEE International Conference on Sustainable Energy Technologies, IEEE, 2008, pp. 1256–1261. <https://doi.org/10.1109/icset.2008.4747199>.
- [10] R. C. Garcia, J. Contreras, M. vanAkkeren, J. B. C. Garcia, A GARCH forecasting model to predict day-ahead electricity prices, *IEEE Trans. Power Syst.* 20 (2005) 867–874. <https://doi.org/10.1109/tpwrs.2005.846044>.
- [11] C. R. Knittel, M. R. Roberts, An empirical examination of restructured electricity prices, *Energy Econ.* 27 (2005) 791–817. <https://doi.org/10.1016/j.eneco.2004.11.005>.
- [12] N. J. Johannessen, M. Kolhe, M. Goodwin, Deregulated electric energy price forecasting in NordPool market using regression techniques, in: 2019 IEEE Sustainable Power and Energy Conference (iSPEC), IEEE, 2019, pp. 1932–1938. <https://doi.org/10.1109/iSPEC48194.2019.8975173>.
- [13] J. Che, J. Wang, Short-term electricity prices forecasting based on support vector regression and auto-regressive integrated moving average modeling, *Energy Convers. Manag.* 51 (2010) 1911–1917. <https://doi.org/10.1016/j.enconman.2010.02.023>.
- [14] F. Feijoo, W. Silva, T. K. Das, A computationally efficient electricity price forecasting model for real time energy markets, *Energy Convers. Manag.* 113 (2016) 27–35. <https://doi.org/10.1016/j.enconman.2016.01.043>.
- [15] J. Mei, D. He, R. Harley, T. Habetler, G. Qu, A random forest method for real-time price forecasting in new york electricity market, in: 2014 IEEE PES General Meeting | Conference & Exposition, IEEE, 2014, pp. 1–5. <https://doi.org/10.1109/PESGM.2014.6939932>.
- [16] A. Lucas, K. Pegios, E. Kotsakis, D. Clarke, Price forecasting for the balancing energy market using machine-learning regression, *Energies* 13 (2020) 5420. <https://doi.org/10.3390/en13205420>.
- [17] S. H. Rafi, Nahid-Al-Masood, M. M. Mahdi, A short-term load forecasting technique using extreme gradient boosting algorithm, in: 2021 IEEE

PES Innovative Smart Grid Technologies - Asia (ISGT Asia), IEEE, 2021, pp. 1–5. <https://doi.org/10.1109/ISGTAsia49270.2021.9715272>.

- [18] Y. Wang, W. Fu, J. Lou, Y. Wang, Z. Li, M. Hu, A comparative study of multiple deep neural network architectures and XGBoost model in electricity price forecasting, in: 2024 5th International Symposium on New Energy and Electrical Technology (ISNEET), IEEE, 2024, pp. 423–430. <https://doi.org/10.1109/isneet64164.2024.10956088>.
- [19] S. Chai, Q. Li, M. Z. Abedin, B. M. Lucey, Forecasting electricity prices from the state-of-the-art modeling technology and the price determinant perspectives, *Res. Int. Bus. Fin.* 67 (2024) 102132. <https://doi.org/10.1016/j.ribaf.2023.102132>.
- [20] M. Lehna, F. Scheller, H. Herwartz, Forecasting day-ahead electricity prices: A comparison of time series and neural network models taking external regressors into account, *Energy Econ.* 106 (2022) 105742. <https://doi.org/10.1016/j.eneco.2021.105742>.
- [21] Y. Wang, H. Wu, J. Dong, Y. Liu, M. Long, J. Wang, Deep time series models: A comprehensive survey and benchmark, *ArXiv* (2024). <https://doi.org/10.48550/arXiv.2407.13278>.
- [22] D. Keles, J. Scelle, F. Paraschiv, W. Fichtner, Extended forecast methods for day-ahead electricity spot prices applying artificial neural networks, *Appl. Energy* 162 (2016) 218–230. <https://doi.org/10.1016/j.apenergy.2015.09.087>.
- [23] W. Li, D. M. Becker, Day-ahead electricity price prediction applying hybrid models of LSTM-based deep learning methods and feature selection algorithms under consideration of market coupling, *Energy* 237 (2021) 121543. <https://doi.org/10.1016/j.energy.2021.121543>.
- [24] K. Prakash, J. G. Singh, Electricity price forecasting using hybrid deep learned networks, *J. Forecast.* 42 (2023) 1750–1771. <https://doi.org/10.1002/for.2981>.
- [25] P.-H. Kuo, C.-J. Huang, An electricity price forecasting model by hybrid structured deep neural networks, *Sustainability* 10 (2018) 1280. <https://doi.org/10.3390/su10041280>.

- [26] C.-J. Huang, Y. Shen, Y.-H. Chen, H.-C. Chen, A novel hybrid deep neural network model for short-term electricity price forecasting, *Int. J. Energy Res.* 45 (2021) 2511–2532. <https://doi.org/10.1002/er.5945>.
- [27] M. Heidarpanah, F. Hooshyaripor, M. Fazeli, Daily electricity price forecasting using artificial intelligence models in the iranian electricity market, *Energy* 263 (2023) 126011. <https://doi.org/10.1016/j.energy.2022.126011>.
- [28] K. Li, Y. Mu, F. Yang, H. Wang, Y. Yan, C. Zhang, Joint forecasting of source-load-price for integrated energy system based on multi-task learning and hybrid attention mechanism, *Appl. Energy* 360 (2024) 122821. <https://doi.org/10.1016/j.apenergy.2024.122821>.
- [29] Y. Q. Tan, Y. X. Shen, X. Y. Yu, X. Lu, Day-ahead electricity price forecasting employing a novel hybrid frame of deep learning methods: A case study in NSW, australia, *Electric Power Syst. Res.* 220 (2023) 109300. <https://doi.org/10.1016/j.epsr.2023.109300>.
- [30] S. Ghimire, R. C. Deo, D. Casillas-Pérez, S. Salcedo-Sanz, Two-step deep learning framework with error compensation technique for short-term, half-hourly electricity price forecasting, *Appl. Energy* 353 (2024) 122059. <https://doi.org/10.1016/j.apenergy.2023.122059>.
- [31] M. Li, X. Wang, Short-term electricity price forecasting via CPO-enhanced dual decomposition and NRBO-optimized deep learning, *Digit. Signal Process.* 168 (2025) 105520. <https://doi.org/10.1016/j.dsp.2025.105520>.
- [32] F. Wang, G. Zhu, T. Pu, D. Xiang, TSGT: Electricity price prediction model based on time-space-GCN-transformer, *Procedia Comput. Sci.* 266 (2025) 357–364. <https://doi.org/10.1016/j.procs.2025.08.045>.
- [33] Z. Deng, X. Qi, T. Xu, Y. Zheng, Operational scheduling of behind-the-meter storage systems based on multiple nonstationary decomposition and deep convolutional neural network for price forecasting, *Comput. Intell. Neurosci.* 2022 (2022) 9326856. <https://doi.org/10.1155/2022/9326856>.
- [34] A. A. A. Khan, M. H. Ullah, R. Tabassum, M. F. Kabir, Enhanced transformer-BiLSTM deep learning framework for day-ahead

energy price forecasting, *IEEE Trans. Ind. Appl.* (2025) 1–15. <https://doi.org/10.1109/tia.2025.3599812>.

[35] S. Perla, R. Bisoi, P. K. Dash, A. K. Rout, Short-term forecasting of electricity price using ensemble deep kernel based random vector functional link network, *Appl. Soft Comput.* 174 (2025) 113012. <https://doi.org/10.1016/j.asoc.2025.113012>.

[36] B. Ehsani, P.-O. Pineau, L. Charlin, Price forecasting in the ontario electricity market via TriConvGRU hybrid model: Univariate vs. multivariate frameworks, *Appl. Energy* 359 (2024) 122649. <https://doi.org/10.1016/j.apenergy.2024.122649>.

[37] J. Lago, F. De Ridder, P. Vrancx, B. De Schutter, Forecasting day-ahead electricity prices in europe: The importance of considering market integration, *Appl. Energy* 211 (2018) 890–903. <https://doi.org/10.1016/j.apenergy.2017.11.098>.

[38] Y. Li, Y. Ding, Y. Liu, T. Yang, P. Wang, J. Wang, W. Yao, Dense skip attention based deep learning for day-ahead electricity price forecasting, *IEEE Trans. Power Syst.* 38 (2022) 4308–4327. <https://doi.org/10.1109/tpwrs.2022.3217579>.

[39] H. Mubarak, A. Abdellatif, S. Ahmad, M. Zohurul Islam, S. M. Muyeen, M. Abdul Mannan, I. Kamwa, Day-ahead electricity price forecasting using a CNN-BiLSTM model in conjunction with autoregressive modeling and hyperparameter optimization, *Int. J. Electr. Power Energy Syst.* 161 (2024) 110206. <https://doi.org/10.1016/j.ijepes.2024.110206>.

[40] H. Chitsaz, P. Zamani-Dehkordi, H. Zareipour, P. P. Parikh, Electricity price forecasting for operational scheduling of behind-the-meter storage systems, *IEEE Trans. Smart Grid* 9 (2018) 6612–6622. <https://doi.org/10.1109/TSG.2017.2717282>.

[41] Z. Deng, C. Liu, Z. Zhu, Inter-hours rolling scheduling of behind-the-meter storage operating systems using electricity price forecasting based on deep convolutional neural network, *Int. J. Electr. Power Energy Syst.* 125 (2021) 106499. <https://doi.org/10.1016/j.ijepes.2020.106499>.

- [42] Z. Chang, Y. Zhang, W. Chen, Electricity price prediction based on hybrid model of adam optimized LSTM neural network and wavelet transform, *Energy* 187 (2019) 115804. <https://doi.org/10.1016/j.energy.2019.07.134>.
- [43] K. Iwabuchi, K. Kato, D. Watari, I. Taniguchi, F. Catthoor, E. Shirazi, T. Onoye, Flexible electricity price forecasting by switching mother wavelets based on wavelet transform and long short-term memory, *Energy and AI* 10 (2022) 100192. <https://doi.org/10.1016/j.egyai.2022.100192>.
- [44] A. Pourdaryaei, M. Mohammadi, H. Mubarak, A. Abdellatif, M. Karimi, E. Gryazina, V. Terzija, A new framework for electricity price forecasting via multi-head self-attention and CNN-based techniques in the competitive electricity market, *Expert Syst. Appl.* 235 (2024) 121207. <https://doi.org/10.1016/j.eswa.2023.121207>.
- [45] Y. Yang, Z. Tan, H. Yang, G. Ruan, H. Zhong, F. Liu, Short-term electricity price forecasting based on graph convolution network and attention mechanism, *IET Renew. Power Gener.* 16 (2022) 2481–2492. <https://doi.org/10.1049/rpg2.12413>.
- [46] B. N. Oreshkin, D. Carpov, N. Chapados, Y. Bengio, N-BEATS: Neural basis expansion analysis for interpretable time series forecasting, in: International Conference on Learning Representations (ICLR), 2020. <https://doi.org/10.48550/arXiv.1905.10437>.
- [47] H. Zhou, S. Zhang, J. Peng, S. Zhang, J. Li, H. Xiong, W. Zhang, Informer: Beyond efficient transformer for long sequence time-series forecasting, in: Proceedings of the Thirty-Fifth AAAI Conference on Artificial Intelligence, volume 35, Association for the Advancement of Artificial Intelligence (AAAI), 2021, pp. 11106–11115. <https://doi.org/10.1609/aaai.v35i12.17325>.
- [48] H. Wu, J. Xu, J. Wang, M. Long, Autoformer: Decomposition transformers with auto-correlation for long-term series forecasting, in: Advances in Neural Information Processing Systems, volume 34, Curran Associates, Inc., 2021, pp. 22419–22430. <https://doi.org/10.48550/arXiv.2106.13008>.

- [49] M. Liu, A. Zeng, M.-H. Chen, Z. Xu, Q. Lai, L. Ma, Q. Xu, SCINet: Time series modeling and forecasting with sample convolution and interaction, in: Advances in Neural Information Processing Systems, volume 35, Curran Associates, Inc., 2022, pp. 5816–5828. <https://doi.org/10.48550/arXiv.2106.09305>.
- [50] A. Gu, K. Goel, C. R'e, Efficiently modeling long sequences with structured state spaces, in: International Conference on Learning Representations (ICLR), 2022. <https://doi.org/10.48550/arXiv.2111.00396>.
- [51] T. Zhou, Z. Ma, Q. Wen, X. Wang, L. Sun, R. Jin, FED-former: Frequency enhanced decomposed transformer for long-term series forecasting, in: Proceedings of the 39th International Conference on Machine Learning, volume 162, PMLR, 2022, pp. 27268–27286. <https://doi.org/10.48550/arXiv.2201.12740>.
- [52] Y. Nie, N. H. Nguyen, P. Sinthong, J. Kalagnanam, A time series is worth 64 words: Long-term forecasting with transformers, in: International Conference on Learning Representations (ICLR), 2023. <https://doi.org/10.48550/arXiv.2211.14730>.
- [53] A. Zeng, M. Chen, L. Zhang, Q. Xu, Are transformers effective for time series forecasting?, in: Proceedings of the Thirty-Seventh AAAI Conference on Artificial Intelligence, volume 37, Association for the Advancement of Artificial Intelligence (AAAI), 2023, pp. 11121–11128. <https://doi.org/10.1609/aaai.v37i9.26317>.
- [54] H. Wu, T. Hu, Y. Liu, H. Zhou, J. Wang, M. Long, TimesNet: Temporal 2D-variation modeling for general time series analysis, in: International Conference on Learning Representations (ICLR), 2023. <https://doi.org/10.48550/arXiv.2210.02186>.
- [55] Y. Liu, T. Hu, H. Zhang, H. Wu, S. Wang, L. Ma, M. Long, iTransformer: Inverted transformers are effective for time series forecasting, in: International Conference on Learning Representations (ICLR), 2024. <https://doi.org/10.48550/arXiv.2310.06625>.
- [56] A. Gu, T. Dao, Mamba: Linear-time sequence modeling with selective state spaces, in: First Conference on Language Modeling, 2024. <https://doi.org/10.48550/arXiv.2312.00752>.

- [57] S. Wang, H. Wu, X. Shi, T. Hu, H. Luo, L. Ma, J. Y. Zhang, J. Zhou, TimeMixer: Decomposable multiscale mixing for time series forecasting, in: International Conference on Learning Representations (ICLR), 2024. <https://doi.org/10.48550/arXiv.2405.14616>.
- [58] Y. Wang, H. Wu, J. Dong, G. Qin, H. Zhang, Y. Liu, Y. Qiu, J. Wang, M. Long, TimeXer: Empowering transformers for time series forecasting with exogenous variables, in: Advances in Neural Information Processing Systems, 2024, p. 469–498. <https://doi.org/10.48550/arXiv.2402.19072>.
- [59] Z. Wang, F. Kong, S. Feng, M. Wang, X. Yang, H. Zhao, D. Wang, Y. Zhang, Is mamba effective for time series forecasting?, Neurocomputing 619 (2025) 129178. <https://doi.org/10.1016/j.neucom.2024.129178>.
- [60] H. Lu, X. Ma, M. Ma, S. Zhu, Energy price prediction using data-driven models: A decade review, Comput. Sci. Rev. 39 (2021) 100356. <https://doi.org/10.1016/j.cosrev.2020.100356>.
- [61] R. J. Hyndman, A. B. Koehler, Another look at measures of forecast accuracy, Int. J. Forecast. 22 (2006) 679–688. <https://doi.org/10.1016/j.ijforecast.2006.03.001>.
- [62] J. Lago, G. Marcjasz, B. De Schutter, R. Weron, Forecasting day-ahead electricity prices: A review of state-of-the-art algorithms, best practices and an open-access benchmark, Appl. Energy 293 (2021) 116983. <https://doi.org/10.1016/j.apenergy.2021.116983>.